PERGAMON

International Journal of Solids and Structures 40 (2003) 3647–3679

INTERNATIONAL JOURNAL OF SOLIDS and STRUCTURES

www.elsevier.com/locate/ijsolstr

Determination of the size of the representative volume element for random composites: statistical and numerical approach

T. Kanit [a], S. Forest [a,*], I. Galliet [a], V. Mounoury [a], D. Jeulin [a,b]

[a] *Centre des Matériaux/UMR 7633, Ecole des Mines de Paris/CNRS, B.P. 87, 91003 Evry, France*

[b] *Centre de Morphologie Mathématique, Ecole des Mines de Paris, 35, Rue St-Honoré, 77305 Fontainebleau, France*

Received 30 March 2002; received in revised form 24 February 2003

Abstract

The representative volume element (RVE) plays a central role in the mechanics and physics of random heterogeneous materials with a view to predicting their effective properties. A quantitative definition of its size is proposed in this work. A RVE size can be associated with a given precision of the estimation of the wanted overall property and the number of realizations of a given volume V of microstructure that one is able to consider. It is shown to depend on the investigated morphological or physical property, the contrast in the properties of the constituents, and their volume fractions. The methodology is applied to a specific random microstructure, namely a two-phase three-dimensional Voronoï mosaic. Finite element simulations of volumes of different sizes are performed in the case of linear elasticity and thermal conductivity. The volumes are subjected to homogeneous strain, stress or periodic boundary conditions. The effective properties can be determined for large volumes and a small number of realizations. Conversely, smaller volumes can be used providing that a sufficient number of realizations are considered. A bias in the estimation of the effective properties is observed for too small volumes for all types of boundary conditions. The variance of computed apparent properties for each volume size is used to define the precision of the estimation. The key-notion of integral range is introduced to relate this error estimation and the definition of the RVE size. For given wanted precision and number of realizations, one is able to provide a minimal volume size for the computation of effective properties. The results can also be used to predict the minimal number of realizations that must be considered for a given volume size in order to estimate the effective property for a given precision. The RVE sizes found for elastic and thermal properties, but also for a geometrical property like volume fraction, are compared.

Keywords: Representative volume element; Homogenization; Random composites; Heterogeneous materials; Microstructure; Integral range; Voronoï mosaic; Finite element; Parallel computing

* Corresponding author. Tel.: +33-1-6076-3051; fax: +33-1-6076-3150.
E-mail address: samuel.forest@ensmp.fr (S. Forest).

0020-7683/03/$ - see front matter © 2003 Elsevier Science Ltd. All rights reserved.
doi:10.1016/S0020-7683(03)00143-4

1. Introduction

One important goal of the mechanics and physics of heterogeneous materials is to derive their effective properties from the knowledge of the constitutive laws and spatial distribution of their components. Homogenization methods have been designed for this purpose. They have reached a high level of sophistication and efficiency, especially in the case of linear properties such as thermal conductivity or elasticity. They can be found in reference extended papers and textbooks like Willis (1981), Sanchez-Palencia and Zaoui (1987) and Nemat-Nasser and Hori (1993) or, more recently, Suquet (1997), Ponte Castañeda and Suquet (1987), Bornert et al. (2001), Besson et al. (2001) and Jeulin and Ostoja-Starzewski (2001), where extensions to nonlinear properties are also proposed.

On the one hand, rigorous bounds for the macroscopic linear properties of composites are available. They include the well-known Voigt and Reuss bounds that take only the volume fraction of the components into account. Hashin and Shtrikman's bounds incorporate the notion of isotropic distribution of phases (Hashin and Shtrikman, 1963). Third order bounds, in the case of random media, were obtained in the general case by Beran (1968), and later for two-phase materials by Miller (1969) and Milton (1982). The incorporation of more and more statistical information on the distribution of heterogeneities in random materials leads to a hierarchy of bounds, as suggested by the systematic theory of Kröner (1980), and also in Torquato and Stell (1983), Torquato and Lado (1986) and Torquato (1991). Note that some of these bounds are optimal in the sense that specific morphologies can be designed that give exactly the value of the bound as effective property.

On the other hand, direct estimations of the wanted effective properties can be proposed. The Mori-Tanaka model for instance favours one phase as a matrix. In contrast, the self-consistent (SC) scheme, presented by Beran (1968) for thermal conductivity and by Hershey (1954) and Kröner (1958) for linear polycrystals, refers to a disordered distribution of phases. A geometrical construction given by Milton (1985) for two-phase composites is obtained by a multiscale stacking of spheres of every phase with the appropriate volume fractions; for this disordered morphology, and for the estimations of the SC model, the role of every component is symmetric.

In all these theories, the proposed estimations are given for random composite media with an infinite extension, and can therefore be denoted as asymptotic estimates. A different way to solve homogenization problems is to use numerical techniques and simulations on samples of the microstructure. In that case, the notion of representative volume element (RVE) is of paramount importance. The RVE is usually regarded as a volume V of heterogeneous material that is sufficiently large to be statistically representative of the composite, i.e., to effectively include a sampling of all microstructural heterogeneities that occur in the composite. This is generally the principle adopted, and it leads to the fact that the RVE must include a large number of the composite microheterogeneities (grains, inclusions, voids, fibers, etc.). It must however remain small enough to be considered as a volume element of continuum mechanics. Several types of boundary conditions can be prescribed on V to impose a given mean strain or mean stress to the material element. As a matter of fact, the response of the RVE must be independent of the type of boundary conditions, as proved by Sab (1992). This also pleads for a rather large size of RVE.

Another definition of the RVE was recently proposed by Drugan and Willis (1996): "*It is the smallest material volume element of the composite for which the usual spatially constant* (*overall modulus*) *macroscopic constitutive representation is a sufficiently accurate model to represent mean constitutive response*". This approach uses the solution of the homogenization for an infinite medium, and does not consider statistical fluctuations of the effective properties over finite domains. In contrast to the large RVE sizes expected from the previous definitions, the estimates of RVE size found by Drugan and Willis (1996) turn out to be much smaller (a small number of fibers for disordered fiber composite for instance).

Numerical techniques can help determining a critical size of volume V and choosing among the previous conflicting definitions. Monte-Carlo simulations were used by Gusev (1997) to generate independent

realizations of disordered distributions of spheres in a matrix. A few dozen of spheres were necessary to obtain small scatter in the averaged property. In Forest et al. (2000), the stress–strain curves of polycrystalline wires in torsion were simulated as a function of the number of grains within the cross-section: about 30 grains in the cross-section were necessary to reach stationary responses. Other examples of convergence of overall properties as the unit cell size is increased can be found in Povirk (1994) and Terada et al. (1998). In Zeman and Sejnoha (2001), the numerical simulations are combined with the use of statistical information like the two-point probability. In Roberts and Garboczi (2000), the finite element method is used to estimate the elastic properties for various models of porous ceramics. Statistical fluctuation is briefly investigated but not related to estimations of RVE sizes. Examples of microstructural dependence of Young's modulus and Poisson's ratio, computed via the finite element method, can be found in Roberts and Garboczi (2001) and Meille and Garboczi (2001).

For microstructures with a high contrast of properties, the bounds are too far apart to give a useful estimate of the effective properties. On the other hand, estimates like the SC model can give a fair prediction but correspond to a very specific morphology of the components. For these reasons, we have to use a numerical method. In the present work, computational homogenization methods are used to determine the effective properties of heterogeneous materials.

In some experiments but also in many simulations, large size volumes V cannot be handled, so that one has to work with apparent moduli obtained on volumes smaller than the RVE. This situation has been extensively studied by Huet (1990) and Hazanov and Huet (1994). Bounding relations between apparent and effective properties are derived for several types of strain, stress or mixed boundary conditions.

The aim of the present work is to propose and illustrate a more quantitative definition of the RVE, which is based on statistical arguments: the RVE must ensure a given accuracy of the estimated property obtained by spatial averaging of the stress, the strain, or the energy fields in a given domain V. Alternatively, the use of smaller volumes V must be compensated by averaging over several realizations of the microstructure to get the same accuracy, provided no bias is introduced in the estimation by some edge effects generated by the boundary conditions. It will appear that the overall moduli obtained by averaging over small domains of composite material, using a sufficient number of realizations for each of the studied boundary conditions, is not the same, in general, as that obtained by a sufficiently large RVE. Note that, in general, the size of a RVE depends on the investigated morphological or physical property. For the same microstructure, it will be shown that the RVE size differs if thermal or elastic properties are considered. It makes sense also to define the notion of RVE for a morphological property like volume fraction. Again, it will appear that the corresponding size is different from that found for a physical property. The key-notion that will be used for a precise definition of the RVE is the integral range classically used in mathematical morphology and recalled in Section 3.2. The notion of integral range has already been used for the homogenization, by simulations, of the elastic properties of 2D random composites, but without explicit reference to the notion of RVE (Cailletaud et al., 1994).

The example of microstructure chosen in this work to illustrate the methodology of determination of RVE is a three-dimensional two-phase Voronoï mosaics. Three-dimensional Voronoï cells are simple representations of grains in a polycrystal and have been used in the past to study the elastoplastic behaviour of polycrystals in Forest et al. (2000), Barbe et al. (2001a) and Barbe et al. (2001b). Here only two phases are considered with a high contrast of properties to enhance the variability of apparent properties on small volumes. Because of the high value of contrast in properties, large volume sizes V must be investigated. The numerical simulations are performed using the finite element method. This means that it will be necessary to use gigantic meshes with a huge amount of degrees of freedom. The resolution is possible only by means of parallel computing.

The representativity of the measurements obtained from limited domains of the random two-phase heterogeneous material, is investigated. These measurements of the specimen concern the morphology (volume fraction), and the following effective physical properties: elastic moduli and thermal conductivity.

The variances of the apparent volume fraction, elastic moduli and thermal conductivity are obtained in windows of increasing sizes. In the paper, the hard phase (respectively highly conductive) is labelled 1, with volume fraction P_1. The soft one (respectively less conductive) is called 2, with volume fraction P_2.

The paper is organized as follows. Section 2 recalls the main definitions, boundary conditions and notations of the whole paper for the determination of effective elastic and thermal properties. A brief statistical description of heterogeneous materials is provided in Section 3 focusing on covariance and integral range. The case of Voronoï mosaics is introduced in Section 3.3. The numerical tools necessary for the Monte-Carlo simulations follow in Section 4 with special attention to the meshing of Voronoï polyhedra, mesh size and parallel computing techniques. The effective properties for this type of microstructure are obtained in Section 5 for volume fraction, elasticity and thermal conductivity. The stress is led on the study of dispersion (variance) as a function of volume size and on the determination of corresponding integral ranges. A quantitative definition of RVE size based on the notion of integral range is introduced in Section 6. The different RVE sizes found for the different properties are compared. Their dependence on volume fraction and contrast of properties is also addressed.

2. Effective linear properties

The elements and notations of homogenization theory necessary for the numerical determination of effective properties carried out in Section 5 are presented below for linear elasticity and for thermal conductivity. Special attention is focused on boundary conditions to be prescribed on volume elements and to the definition of effective and apparent properties. More details and the proofs of the given results can be found in the textbooks and reference articles mentioned at the beginning of the introduction.

2.1. Linear elasticity

A volume element V made of heterogeneous material is considered. Conditions are prescribed at its boundary ∂V in order to estimate its overall properties.

2.1.1. Boundary conditions

In this work, three types of boundary conditions to be prescribed on individual volume element V are considered:

- Kinematic uniform boundary conditions (KUBC): The displacement $\underline{u}$ is imposed at point $\underline{x}$ belonging to the boundary ∂V such that:

$$\underline{u} = \underset{\sim}{E} \cdot \underline{x} \quad \forall \underline{x} \in \partial V \tag{1}$$

  $\underset{\sim}{E}$ is a symmetrical second-rank tensor that does not depend on $\underline{x}$. This implies that:

$$\langle \underset{\sim}{\varepsilon} \rangle \hat{=} \frac{1}{V} \int_V \underset{\sim}{\varepsilon} \, \mathrm{d}V = \underset{\sim}{E} \tag{2}$$

  The sign $\hat{=}$ means a definition of the left quantity. The macroscopic stress tensor is then defined by the spatial average:

$$\underset{\sim}{\Sigma} \hat{=} \langle \underset{\sim}{\sigma} \rangle = \frac{1}{V} \int_V \underset{\sim}{\sigma} \, \mathrm{d}V \tag{3}$$

- Static uniform boundary conditions (SUBC): The traction vector is prescribed at the boundary:

$$\underset{\sim}{\sigma} \cdot \underline{n} = \underset{\sim}{\Sigma} \cdot \underline{n} \quad \forall \underline{x} \in \partial V \tag{4}$$

$\underset{\sim}{\Sigma}$ is a symmetrical second-rank tensor independent of $\underline{x}$. The vector normal to ∂V at $\underline{x}$ is denoted by $\underline{n}$. This implies that:

$$\langle \underset{\sim}{\sigma} \rangle \hat{=} \frac{1}{V} \int_V \underset{\sim}{\sigma} \mathrm{d}V = \underset{\sim}{\Sigma} \tag{5}$$

The macroscopic strain tensor is then defined as the spatial average:

$$\underset{\sim}{E} \hat{=} \langle \underset{\sim}{\varepsilon} \rangle = \frac{1}{V} \int_V \underset{\sim}{\varepsilon} \mathrm{d}V \tag{6}$$

- Periodicity conditions (PERIODIC): The displacement field over the entire volume V takes the form

$$\underline{u} = \underset{\sim}{E} \cdot \underline{x} + \underline{v} \quad \forall \underline{x} \in V \tag{7}$$

where the fluctuation $\underline{v}$ is periodic. It takes the same values at two homologous points on opposite faces of V. The traction vector $\underset{\sim}{\sigma} \cdot \underline{n}$ takes opposite values at two homologous points on opposite faces of V.

When the constitutive behaviour of the components is described by linear elasticity, each micromechanical problem (KUBC, SUBC and PERIODIC) admits a single solution, up to a rigid body motion for problem SUBC and a translation for PERIODIC. Accordingly, there exists a four-rank concentration tensor field $\underset{\approx}{A}$ such that:

$$\underset{\sim}{\varepsilon}(\underline{x}) = \underset{\approx}{A}(\underline{x}) : \underset{\sim}{E} \quad \forall \underline{x} \in V \quad \text{and} \quad \forall \underset{\sim}{E} \tag{8}$$

for the KUBC problem, and a four-rank concentration tensor field $\underset{\approx}{B}$ such that:

$$\underset{\sim}{\sigma}(\underline{x}) = \underset{\approx}{B}(\underline{x}) : \underset{\sim}{\Sigma} \quad \forall \underline{x} \in V \quad \text{and} \quad \forall \underset{\sim}{\Sigma} \tag{9}$$

for the SUBC problem. From Eqs. (3) and (6), the concentration tensors satisfy:

$$\langle \underset{\approx}{A} \rangle = \langle \underset{\approx}{B} \rangle = \underset{\approx}{I} \tag{10}$$

$\underset{\approx}{I}$ is the fourth-rank identity tensor operating on symmetric second-rank tensors.

2.1.2. Apparent and effective moduli

Let $\underset{\approx}{c}(\underline{x})$ and $\underset{\approx}{s}(\underline{x})$ be the four-rank tensor fields of elastic moduli and compliances in the volume V of heterogeneous material:

$$\underset{\sim}{\sigma}(\underline{x}) = \underset{\approx}{c}(\underline{x}) : \underset{\sim}{\varepsilon}(\underline{x}), \quad \underset{\sim}{\varepsilon}(\underline{x}) = \underset{\approx}{s}(\underline{x}) : \underset{\sim}{\sigma}(\underline{x}) \quad \forall \underline{x} \in V \tag{11}$$

For the KUBC problem, one has then:

$$\underset{\sim}{\Sigma} = \langle \underset{\sim}{\sigma} \rangle = \langle \underset{\approx}{c} : \underset{\approx}{A} : \underset{\sim}{E} \rangle = \langle \underset{\approx}{c} : \underset{\approx}{A} \rangle : \underset{\sim}{E} = \underset{\approx}{C}_E^{\mathrm{app}} : \underset{\sim}{E} \tag{12}$$

and for the SUBC problem:

$$\underset{\sim}{E} = \langle \underset{\sim}{\varepsilon} \rangle = \langle \underset{\approx}{s} : \underset{\approx}{B} : \underset{\sim}{\Sigma} \rangle = \langle \underset{\approx}{s} : \underset{\approx}{B} \rangle : \underset{\sim}{\Sigma} = \underset{\approx}{S}_\Sigma^{\mathrm{app}} : \underset{\sim}{\Sigma} \tag{13}$$

which defines unambiguously apparent moduli $\underset{\approx}{C}_E^{\mathrm{app}}$ and apparent compliances $\underset{\approx}{S}_\Sigma^{\mathrm{app}}$ for a given volume V. The relations show that the apparent properties are not given in general by a simple law of mixtures, but involve a more complex averaging process.

A definition of apparent moduli based on strain energy e is also possible:

$$e \hat{=} \langle \underset{\sim}{\sigma} : \underset{\sim}{\varepsilon} \rangle = \langle \underset{\sim}{\varepsilon} : \underset{\approx}{c} : \underset{\sim}{\varepsilon} \rangle = \underset{\sim}{E} : \langle \underset{\approx}{A}^{\mathrm{T}} : \underset{\approx}{c} : \underset{\approx}{A} \rangle : \underset{\sim}{E} \tag{14}$$

for the KUBC problem, and:

$$e = \langle \underset{\sim}{\sigma} : \underset{\sim}{\varepsilon} \rangle = \langle \underset{\sim}{\sigma} : \underset{\approx}{s} : \underset{\sim}{\sigma} \rangle = \underset{\sim}{\Sigma} : \langle \underset{\approx}{B}^{\mathrm{T}} : \underset{\approx}{s} : \underset{\approx}{B} \rangle : \underset{\sim}{\Sigma} \tag{15}$$

for the SUBC problem. The exponent 'T' denotes transposition. This leads to the following definition of apparent moduli:

$$\underset{\approx}{C}_E^{\mathrm{app}} = \langle \underset{\approx}{A}^{\mathrm{T}} : \underset{\approx}{c} : \underset{\approx}{A} \rangle, \quad \underset{\approx}{S}_{\Sigma}^{\mathrm{app}} = \langle \underset{\approx}{B}^{\mathrm{T}} : \underset{\approx}{s} : \underset{\approx}{B} \rangle \tag{16}$$

The symmetry of the apparent moduli is clearer in these formula. However the application of so-called Hill-Mandel lemma shows that both definitions are in fact equivalent (Sanchez-Palencia and Zaoui, 1987).

For sufficiently large volumes V, the apparent moduli do not depend any more on the type of boundary conditions and coincide with the wanted effective properties of the medium (Sab, 1992):

$$\underset{\approx}{C}_E^{\mathrm{app}} = \underset{\approx}{S}_{\Sigma}^{\mathrm{app\text{-}1}} = \underset{\approx}{C}^{\mathrm{eff}} = \underset{\approx}{S}^{\mathrm{eff\text{-}1}} \tag{17}$$

For intermediate volumes V, one simply has the following bounding inequations (Huet, 1990):

$$\underset{\approx}{S}_{\Sigma}^{\mathrm{app\text{-}1}} \leqslant \underset{\approx}{C}^{\mathrm{eff}} \leqslant \underset{\approx}{C}_E^{\mathrm{app}} \tag{18}$$

The inequalities must be understood in the sense of quadratic forms. In the computations presented in Section 5.1.2, it will be checked that these relations hold. The periodic estimation for a given volume V also lies between $\underset{\approx}{S}_{\Sigma}^{\mathrm{app\text{-}1}}$ and $\underset{\approx}{C}_E^{\mathrm{app}}$.

2.1.3. Elementary problems on V for isotropic effective properties

Specific boundary value problems are defined in this subsection that will be used for the determination of isotropic effective elastic properties in Section 5.1.2. These are special cases of the previous KUBC, SUBC and PERIODIC conditions, for which specific values of $\underset{\sim}{E}$ and $\underset{\sim}{\Sigma}$ are chosen.

In the case of KUBC and PERIODIC conditions prescribed to a given volume V, one takes

$$\underset{\sim}{E}_k = \begin{pmatrix} \frac{1}{3} & 0 & 0 \\ 0 & \frac{1}{3} & 0 \\ 0 & 0 & \frac{1}{3} \end{pmatrix}, \qquad \underset{\sim}{E}_{\mu} = \begin{pmatrix} 0 & \frac{1}{2} & 0 \\ \frac{1}{2} & 0 & 0 \\ 0 & 0 & 0 \end{pmatrix} \tag{19}$$

An "apparent bulk modulus" k^{app} and an "apparent shear modulus" μ^{app} can be defined as:

$$k^{\mathrm{app}} \hat{=} e(\underset{\sim}{E}_k) = \langle \underset{\sim}{\sigma} \rangle : \underset{\sim}{E}_k = \tfrac{1}{3}\mathrm{trace}\ \langle \underset{\sim}{\sigma} \rangle \tag{20}$$

$$\mu^{\mathrm{app}} \hat{=} e(\underset{\sim}{E}_{\mu}) = \langle \underset{\sim}{\sigma} \rangle : \underset{\sim}{E}_{\mu} = \langle \sigma_{12} \rangle \tag{21}$$

In the case of SUBC boundary conditions, one takes:

$$\underset{\sim}{\Sigma}_k = \begin{pmatrix} 1 & 0 & 0 \\ 0 & 1 & 0 \\ 0 & 0 & 1 \end{pmatrix}, \qquad \underset{\sim}{\Sigma}_{\mu} = \begin{pmatrix} 0 & 1 & 0 \\ 1 & 0 & 0 \\ 0 & 0 & 0 \end{pmatrix} \tag{22}$$

In this case an "apparent bulk modulus" k^{app} and an "apparent shear modulus" μ^{app} can also be defined as:

$$\frac{1}{k^{\mathrm{app}}} \hat{=} e(\underset{\sim}{\Sigma}_k) = \underset{\sim}{\Sigma}_k : \langle \underset{\sim}{\varepsilon} \rangle = \mathrm{trace} \langle \underset{\sim}{\varepsilon} \rangle \tag{23}$$

$$\frac{1}{\mu^{\text{app}}} \hat{=} e(\underset{\sim}{\Sigma}_\mu) = \underset{\sim}{\Sigma}_\mu : \langle \underset{\sim}{\varepsilon} \rangle = 2\langle \varepsilon_{12} \rangle \tag{24}$$

The physical meaning of these quantities is actually that of bulk and shear moduli only when the response of volume V is isotropic, which is generally not the case. The problem of the determination of isotropic apparent moduli from simulations on small volumes is discussed in Section 5.1.2.

2.2. Thermal conductivity

For the thermal problem, the temperature, its gradient and the heat flux vector are denoted by T, ∇T and $\underline{q}$ respectively. The heat flux vector and the temperature gradient are related by Fourier's law, that reads:

$$\underline{q} = \lambda \nabla T \tag{25}$$

in the isotropic case. The scalar λ is the thermal conductivity coefficient of the considered phase.

A volume V of heterogeneous material is considered again. Three types of boundary conditions are used in the study of the effective thermal conductivity:

- Uniform gradient of temperature at the boundary (UGT):

$$T = \underline{G} \cdot \underline{x} \quad \forall \underline{x} \in \partial V \tag{26}$$

$\underline{G}$ is a constant vector independent of $\underline{x}$. This implies that:

$$\langle \nabla T \rangle = \frac{1}{V} \int_V \nabla T \, \mathrm{d}V = \underline{G} \tag{27}$$

The macroscopic flux vector is defined by the spatial average:

$$\underline{Q} \hat{=} \langle \underline{q} \rangle = \frac{1}{V} \int_V \underline{q} \, \mathrm{d}V \tag{28}$$

- Uniform heat flux at the boundary (UHF):

$$\underline{q} \cdot \underline{n} = \underline{Q} \cdot \underline{x} \quad \forall \underline{x} \in \partial V \tag{29}$$

$\underline{Q}$ is a constant vector independent of $\underline{x}$. This implies that:

$$\langle \underline{q} \rangle = \frac{1}{V} \int_V \underline{q} \, \mathrm{d}V = \underline{Q} \tag{30}$$

The macroscopic temperature gradient is given by the spatial average:

$$\underline{G} \hat{=} \langle \nabla T \rangle = \frac{1}{V} \int_V \nabla T \, \mathrm{d}V \tag{31}$$

- Periodic boundary conditions (PERIODIC): the temperature field takes the form

$$T = \underline{G} \cdot \underline{x} + t \quad \forall \underline{x} \in V \tag{32}$$

The fluctuation temperature t is periodic.

Concentration tensors $\underset{\sim}{A}$ and $\underset{\sim}{B}$ exist such that:

$$\nabla T(\underline{x}) = \underset{\sim}{A}(\underline{x}) \cdot \underline{G}, \quad \text{and} \quad \underline{q}(\underline{x}) = \underset{\sim}{B}(\underline{x}) \cdot \underline{Q} \tag{33}$$

for the problems UGT and UHF respectively. Apparent conductivity tensors can be defined as:

$$\underset{\sim}{\lambda}_G^{\text{app}} = \langle \lambda \underset{\sim}{A} \rangle \quad \text{and} \quad \underset{\sim}{\lambda}_Q^{\text{app-1}} = \left\langle \frac{1}{\lambda} \underset{\sim}{B} \right\rangle \tag{34}$$

Apparent conductivities coincide with the wanted effective properties for sufficiently large volumes V.

In the case of isotropic effective properties, as considered in Section 5.1.3, the following test temperature gradient and flux will be prescribed:

$$\underline{G}_\lambda = (1\,1\,1)^{\mathrm{T}} \quad \text{and} \quad \underline{Q}_\lambda = (1\,1\,1)^{\mathrm{T}} \tag{35}$$

They are used respectively to define the following "apparent conductivities":

$$\lambda^{\text{app}} = \tfrac{1}{3}\text{trace}\langle \underline{q} \rangle, \qquad \lambda^{\text{app-1}} = \tfrac{1}{3}\text{trace}\langle \nabla T \rangle \tag{36}$$

3. Statistical description of random heterogeneous media

Models of random media may be useful at two different levels: to provide a description of the heterogeneous structure, and to predict some macroscopic properties of materials. In this part, basic morphological tools that are available to quantitatively characterize the geometry of random media are introduced. They can be easily obtained from the analysis of images of the microstructure. They are illustrated in the last subsection by an estimation of the integral range for a Voronoï mosaic model.

3.1. Reminder on the covariance of a random set

To describe the geometrical dispersion, the state of two points x_1 and x_2 with the separation h can be tested, without considering what happens between the two points (Matheron, 1971; Jeulin, 1981; Serra, 1982; Coster and Chermant, 1989; Jeulin, 2001). The morphological approach based on the covariance is, in general, suitable to study the dispersion.

The covariogram $K(X,h)$ is the measure 'Mes' of the intersection of the set X (surface in $2D$, volume in $3D$) and of the translated set of X by $-h$, X_{-h}. We have:

$$K(X,h) = \text{Mes}(X \cap X_{-h}) = \int k(x)k(x+h)\,\mathrm{d}x \tag{37}$$

$k(x)$ is defined as:

$$k(x) = \begin{cases} 1 & \text{if } x \in X \\ 0 & \text{else} \end{cases}$$

Properties of the covariogram

- For $h = 0$, we have:

$$K(X,0) = \text{Mes}(X \cap X_{-0}) = \text{Mes}(X) \tag{38}$$

- For a bounded set X:

$$K(X,\infty) = 0, \quad K(X,h) = 0 \text{ for } h > A \tag{39}$$

A is the largest distance between two points in X in the direction of h.

- The integral of the covariogram is given by:

$$\int_{R^n} K(X,h)\,\mathrm{d}h = (\text{Mes}(X))^2 \tag{40}$$

The probabilistic version of the covariogram for a stationary set X is the covariance function, noted $C(X,h)$. The covariance function is the probability for the two points x and $x+h$ to be in the set X:

$$C(X,h) = P\{x \in X, x+h \in X\} \tag{41}$$

If X is defined in R^3:

$$C(X,0) = V_V(X) = P \tag{42}$$

V_V is the volume fraction of X in $\mathbf{R}^3$. One has also:

$$C(X,h) = C(X,-h) \leqslant C(X,0) \tag{43}$$

and:

$$\lim_{h\to\infty} C(X,h) = (V_V(X))^2 \tag{44}$$

The covariance presents an asymptotic theoretical value equal to the square of the volume fraction of X.

If this limit is reached before $h \to \infty$, for example, for a value $h = A$, the points of the structure with a distance larger than A are not correlated (Matheron, 1971; Jeulin, 1981; Serra, 1982; Jeulin, 2001). This distance is the range of the covariance. We can estimate the covariance from images (like plane sections) inside a mask, by means of the geometrical covariogram (two examples are given in Fig. 1). The covariance is characteristic of the size and of the arrangement of connected objects building the set X. In Fig. 1a the range is close to 37 μm, while in Fig. 1b it is close to 19 μm, the range for the coarse microstructure being larger than for the fine microstructure. In addition, from the measurement of the covariance in two orthogonal directions given in Fig. 1, it can be seen that the microstructure is isotropic.

3.2. Notion of integral range

It is possible to define a range which gives information on the domain size of the structure for which the parameters measured in this volume have a good statistical representativity. This range is called the integral range (Matheron, 1971, 1975, 1989; Lantuéjoul, 1991; Cailletaud et al., 1994; Jeulin, 2001). The definition of the integral range in the space R^n is:

$$A_n = \frac{1}{C(X,0) - C(X,0)^2} \int_{R^n} (C(X,h) - C(X,0)^2)\,\mathrm{d}h \tag{45}$$

This notion is very useful to predict the variability of properties of a material as a function of the geometry of parts. For instance, the variance $D_P^2(V_V^*)$ of the volume fraction $V_V^* = \mathrm{Mes}(X \cap V)/\mathrm{Mes}\,V$ of a sample with volume V in an infinite domain, for a microstructure with the covariance $C(X,h)$ is given by Matheron (1971):

$$D_P^2(V_V^*) = \frac{1}{V^2} \int_V \int_V (C(X,x-y) - P^2)\,\mathrm{d}x\,\mathrm{d}y \tag{46}$$

For a large specimen ($V \gg A_n$), $D_P^2(V)$ can be expressed as a function of the integral range in the space R^n, A_n, by:

$$D_P^2(V) = \frac{P(1-P)A_n}{V} \tag{47}$$

Therefore, the specimen V is statistically equivalent to $N \simeq V/A_n$ uncorrelated samples. From the variance, it is easy to work out the confidence interval of the average of the volume fraction P ($P \pm 2D_P(V)$) as a function of the volume V and of the integral range. This gives the relative precision of the estimation. Conversely, the volume V to be used to get a given precision is obtained as a function of P and of A_n.

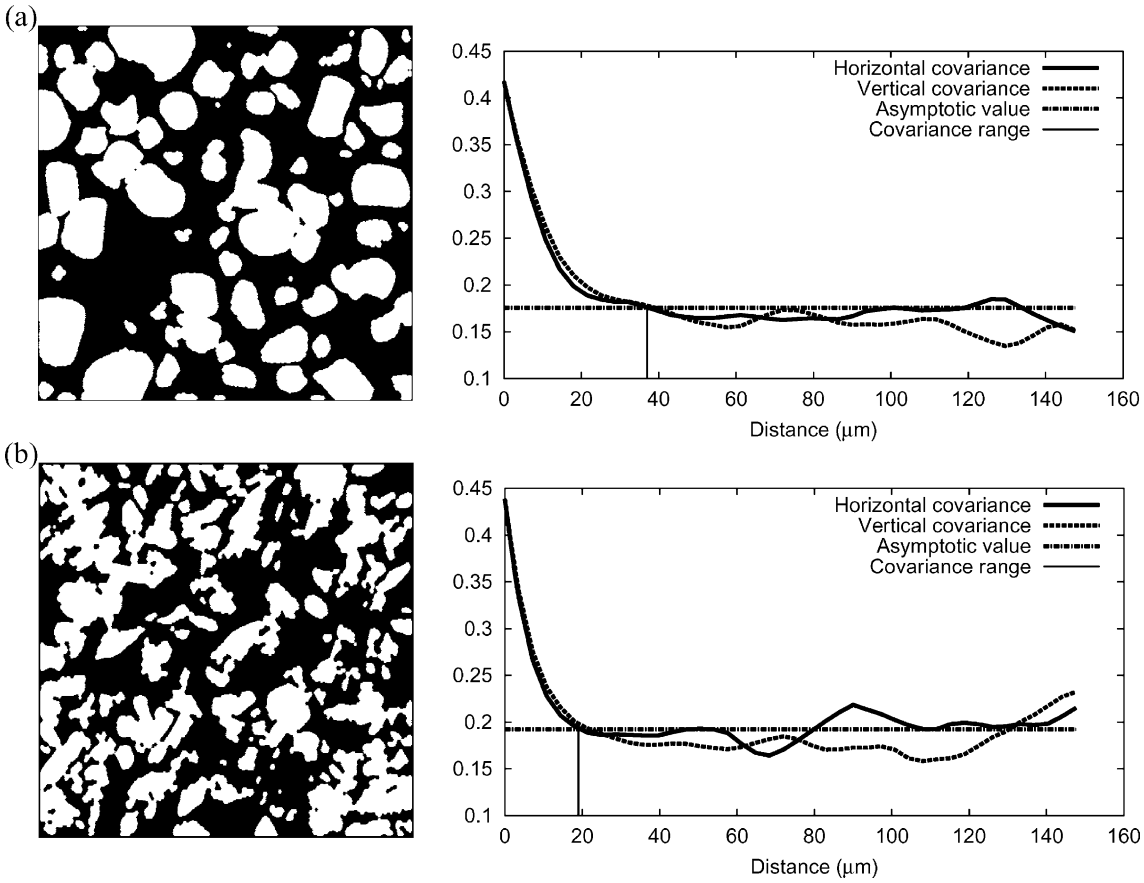

Fig. 1. Microstructures (with the same volume fraction and different morphologies) and their covariances in horizontal and vertical directions; the image size is 150 μm×150 μm. The asymptotic value is equal to the square of the volume fraction (of the white phase); for the fine (a) and coarse (b) microstructures (material from food industry, Colworth, 2000).

This is the reason for interpreting A_n as the scale of the phenomenon, V being the scale of observation. The integral range A_n is a good measure of the notion of scale. It is a convenient measurement of the size of a RVE of a stationary and ergodic random structure.

3.3. Case of the Voronoï mosaic

The previous notions of mathematical morphology can be illustrated in the case of the microstructure considered in the numerical simulations of this work, namely 3D Voronoï mosaics.

To generate such microstructures, an original method is proposed, with numerous extensions of the classical model (Decker and Jeulin, 2000). Its main advantage, as compared to standard procedures, is to generate textures with very large numbers of grains, at a low computational cost.

First pick points $M_1, M_2, \ldots$ in space at random according to a Poisson process of density ρ points per unit volume. Next subdivide space into cells (crystals) $C_1, C_2, \ldots$ by the rule: C_i contains all points in space closer to M_i than to any M_i $(j \neq i)$. In the cell model C_i is a convex polyhedron because it is the intersection

of several half-spaces (points closer to M_i than to M_j form a half-space). M_i will be called the center of C_i. This builds a Voronoï tessellation of space (Gilbert, 1962).

In practice M_i represents the location of the original seed crystal from which C_i grew. One assumes:

(i) the seeds for all crystals start growing at the same instant,
(ii) seeds grow at the same rate in all directions,
(iii) seeds remain fixed in space without pushing apart as they grow into contact (see Fig. 2a).

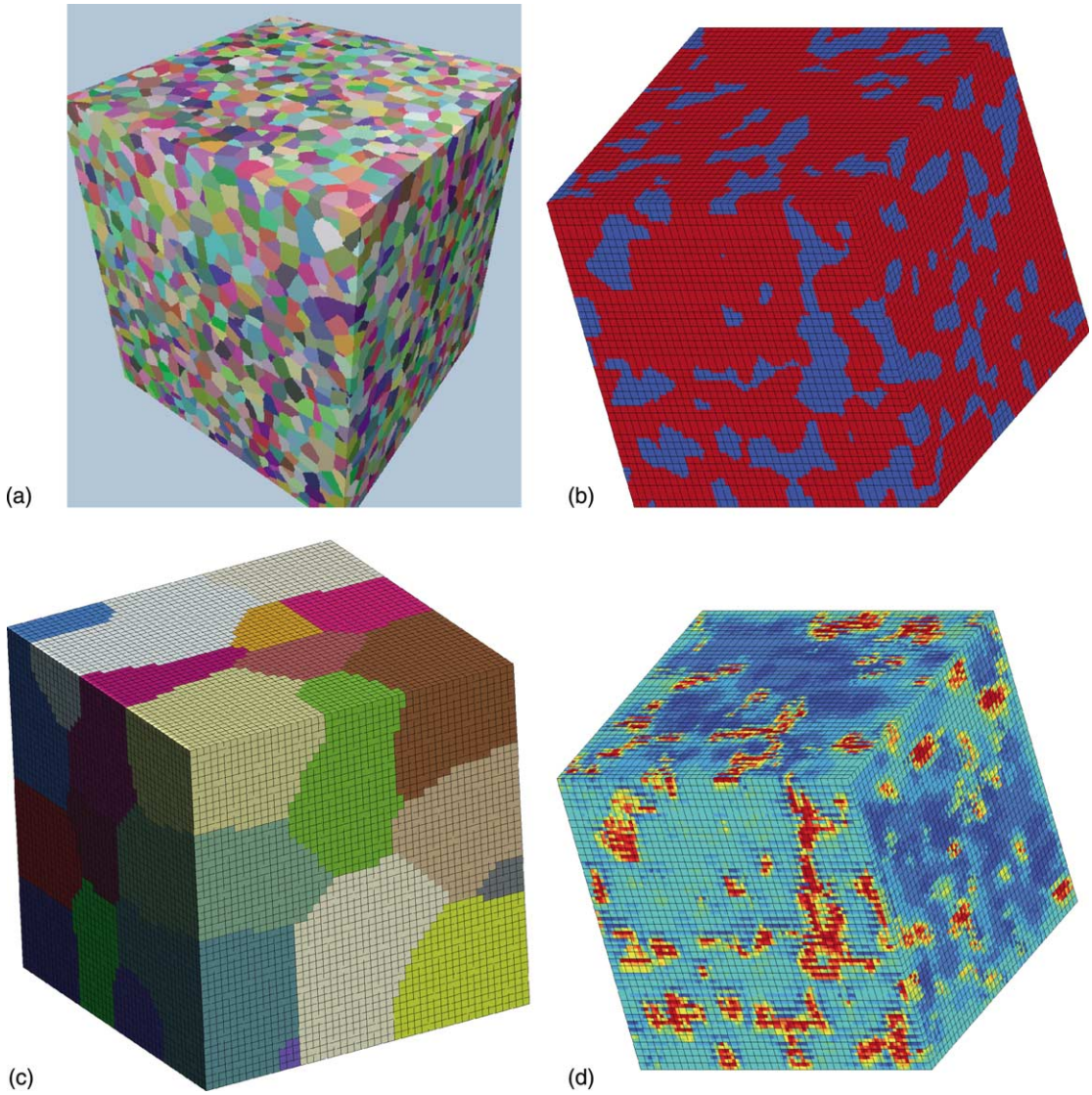

Fig. 2. Voronoï mosaic model and finite element computations: (a) random distribution of 8000 grains in space; (b) image of the same microstructure with two phases distributed randomly among the grains for a given volume fraction of phase 1, with the superimposed finite element mesh; (c) subdivision of the microstructure into 32 subdomains for parallel computing and (d) example of computation of the effective shear modulus with boundary conditions KUBC (von Mises equivalent strain distribution for prescribed mean strain $E_{12} = 0.1$).

Coloring every cell C of the tessellation at random generates a random Voronoï mosaic. In what follows, the colors will in fact correspond to the physical properties of the components of a random composite. To study two-phase materials, two colors are used.

Note that it is possible to superimpose a constraint of periodicity at the boundary of the volume in the generation of the Voronoï mosaic (Decker and Jeulin, 2000; Forest et al., 2000). In the simulations of this paper with periodic boundary conditions, such periodic Voronoï mosaics are used.

In the case of the Voronoï mosaic model, the covariance $C(h)$ of the composite and covariogram $K(h)$ of the random cell C are related by the following equation (Jeulin, 1981):

$$C(h) = P(1-P)\frac{K(h)}{K(0)} + P^2 \tag{48}$$

From the definition of the integral range (Eq. (45)):

$$A_3 = \frac{1}{P(1-P)} \int (C(h) - P^2)\,\mathrm{d}h = \int_{R^3} \frac{K(h)}{K(0)}\,\mathrm{d}h \tag{49}$$

Finally, one obtains:

$$A_3 = \frac{E\{V^2\}}{E\{V\}} \tag{50}$$

$E\{Z\}$ is the mathematical expectation of property Z. The value of the integral range in the case of the Voronoï mosaic model is deduced from the variance of the volume of the random cell C given by Gilbert (1962):

$$A_3 = 1.179 \tag{51}$$

4. Numerical tools for the homogenization

The finite element method is chosen for the computations presented in this work. This requires meshing techniques for microstructures. They are described in Section 4.1. The question of mesh refinement is also discussed here. Section 4.2 presents the parallel computing tools that are necessary to handle large enough meshes.

4.1. Finite element meshing of microstructures

4.1.1. Free mesh and multi-phase elements

Two types of meshes were used and compared in the case of the Voronoï mosaic: the multi-phase element technique and free meshing with tetrahedral elements. Fig. 3 shows them in the case of an aggregate of 20 Voronoï cells. In the multi-phase element technique, an image of the microstructure is used to attribute the proper phase property to each integration point of a regular mesh, according to the color of the underlying voxel. Fig. 3a shows an example of regular mesh with linear eight-node elements and eight integration points per finite element. The main drawback of this simple technique is that in the same finite element two different phases can be present. The element edges do not necessarily follow the interfaces of grains in the microstructure. Such meshes have been used extensively in Lippmann et al. (1997) and Barbe et al. (2001a). The second type is the free meshing technique with tetrahedral elements (see Fig. 3b; Thompson et al., 1999). The faces of all Voronoï cells are meshed using two-dimensional Delaunay triangles. After that, the individual cell volumes are meshed with tetrahedral elements with the constraint that they are built on the 2D meshes of the faces. Accordingly, all integration points of one element belong to the same phase. This

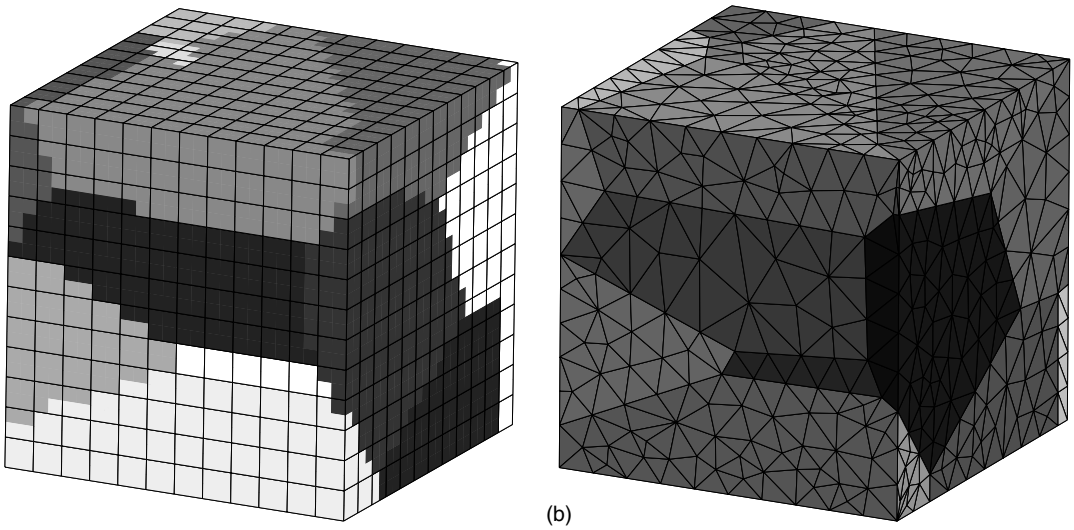

Fig. 3. Two meshes of the same microstructure (20 Voronoï cells) with approximatively the same number of integration points (i.p.) and the same number of degrees of freedom (dof): (a) multi-phase elements (13,824 i.p. and 6591 dof) and (b) free meshing (10,326 i.p. and 6387 dof).

technique usually leads to larger numbers of elements. Both methods are compared in Lippmann et al. (1997) for inclusion-matrix microstructures. Note that Ghosh and Moorthey (1995) developed a finite element method based on Voronoï cells.

For illustration, an example of tensile test is computed in linear elasticity (traction load is prescribed on one face, the opposite one is fixed and all the other faces are free of forces). Phases 1 and 2 were randomly distributed among the 20 grains of Fig. 3 according to a volume fraction of 70% of hard phase P_1. The contrast in Young's modulus is 100 ($E_1 = 2500$ MPa, $E_2 = 25$ MPa) and the Poisson ratio is ($\nu_1 = 0.3$, $\nu_2 = 0.49$). The obtained average stress and strain are found to be identical for both meshes. However slight differences exist for the local fields. The local distributions of von Mises stress are compared in Fig. 4. The local differences are also explained by the insufficient mesh density used in each case. As a result, and for the sake of simplicity, the multi-phase element technique is used in the sequel. Quadratic bricks with reduced integration (20 nodes and eight integration points per element) are used in all following simulations, contrary to the simple previous test. Since only 3D simulations are presented, the number of degrees of freedom in one brick is 60 (the number of nodes multiplied by the three components of displacement at each node). For a large regular cubic grid made of 20-node bricks, the number of nodes is approximately equal to four times the number of bricks. The total number of degrees of freedom is then three times the number of nodes.

4.1.2. Determination of the mesh density

The effect of the mesh density (average number of finite elements used to mesh one Voronoï cell) is studied. Three microstructures of 1000 grains are used for three different volume fractions (72.5%, 66.7% and 52.5% of phase P_1). The material properties are the same as in the previous subsection. Tensile tests are simulated. The number of cells and the geometry of the microstructure is unchanged but different mesh resolutions are used. The number of finite elements was changed from 1728 to 85,184 (the corresponding number of degrees of freedom was changed from 24,843 to 1,075,275). The results given in Fig. 5 show the convergence of the apparent Young's modulus as a function of the number of degrees of freedom. This figure also shows that one must use about 50 quadratic elements to mesh one grain, for the variation of the overall effective elastic response to be smaller than 1%. In the sequel, about 14 finite elements per grain were

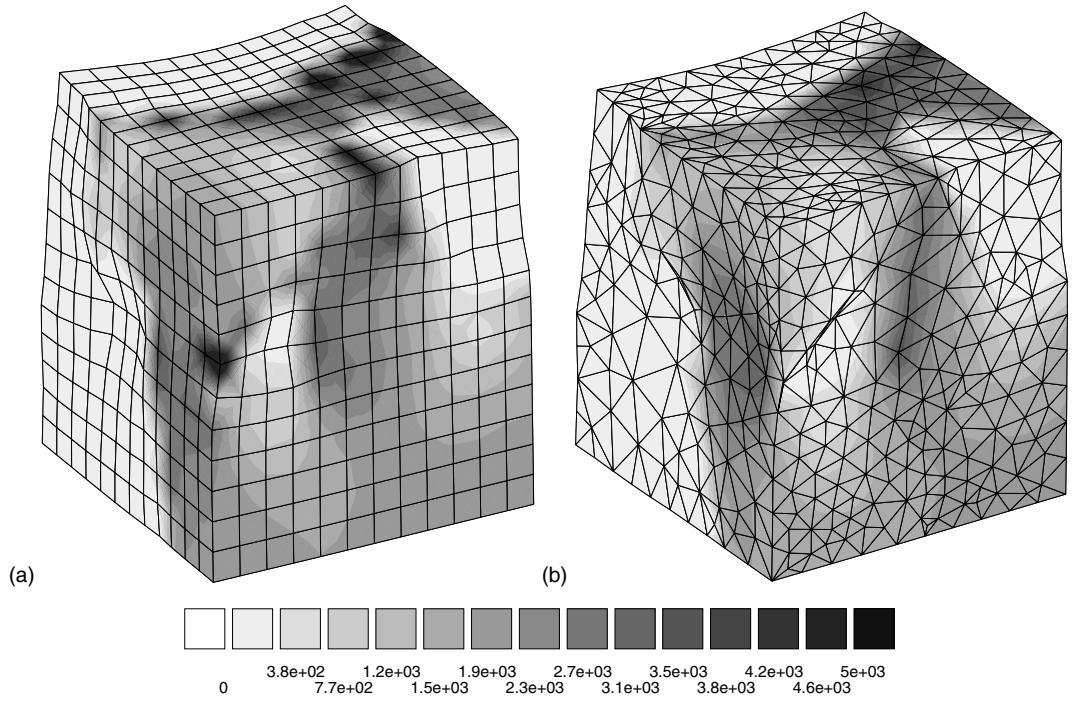

Fig. 4. Distribution of von Mises equivalent stress (MPa) for mean tensile deformation $E_{33} = 0.1$ in vertical direction: (a) multi-phase elements and (b) free mesh.

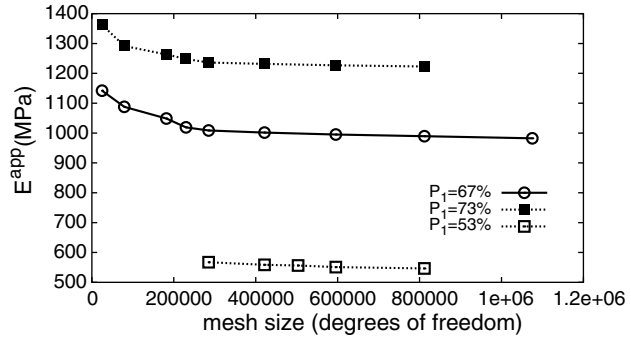

Fig. 5. Effect of mesh size and of the volume fraction of hard phase ($P_1 = P$) on the value of apparent Young's modulus.

retained as mesh density, which corresponds to a precision better than 5% in the results. It has been checked also that this mesh density is sufficient to get a precision better than 1% on the statistical fluctuations and variance of the results when many realizations are considered.

4.2. Parallel computing

In order to characterize the size of the RVE, one must be able to carry out computations with a very large amount of finite elements. For that purpose, we have chosen to resort to parallel computation.

The retained method is the FETI solver (Finite Element Tearing and Interconnecting method (Fahrat and Roux, 1994; Feyel et al., 1997; Feyel, 1998)), which is a dual subdivision method well-known for its numerical scalability. Subdivision means the process of dividing a large finite element mesh into subdomains. The large algebraic system is replaced by a succession of smaller ones related to the subdomains and to the interface between the subdomains. The numerical scalability of FETI allows us to solve problems with a large number of subdomains. The individual problems on subdomains are computed simultaneously on different processors. For a good speed-up, subdivision must give the same amount of work to all processors which must have the same velocity. The aim of the interface problem is to ensure continuity of displacement at the interface between subdomains. FETI is called dual method because the interface problem is posed in terms of forces that glue the subdomains. This interface problem is solved iteratively by a conjugate gradient method.

The large contrast of properties considered in this work can lead to ill-conditioned matrices. This numerical difficulty is solved by using a conjugate gradient algorithm with a preconditioning procedure. Unfortunately, the preconditioning is less efficient for an increasing number of subdomains.

A cluster of 32 PC under Linux was available for the computations of this work. The largest volume computed in this work, in the case of linear elasticity, is a cube with $48 \times 48 \times 48 = 110{,}592$ quadratic bricks for the mesh of about 8000 Voronoï cells (i.e. about 14 elements per cell). This corresponds to almost 1.4 million of degrees of freedom. This mesh and the distribution of the two phases are shown in Fig. 2b. The mesh is decomposed into 32 subdomains (see Fig. 2c). The resolution of the linear elastic problem is done in one single increment, using a multi-frontal solver. About 850 Mo RAM memory are necessary for each processor, so that the whole resolution requires more than 27 Go memory. The entire computation time for one resolution (reading of the mesh, parallel resolution, writing of the output files) is about 1 h and 30 min. An example of result is shown in the case of a shear test with KUBC conditions in Fig. 2d.

5. Determination of morphological and effective physical properties of a two-phase Voronoï mosaic

Three types of overall properties are studied in this part for a large range of volume sizes V and a large number of realizations of the random microstructures. The first one is a geometrical property, namely the overall volume fraction P^{app}. The motivation for studying this simple property stems from the fact that the integral range is known in the case of the Voronoï mosaic (see Eq. (51)). This is a good test for the random generation procedure of the microstructure. Furthermore, this illustrates in a simple way the methodology proposed in this work. The investigated physical properties are the elastic moduli (bulk modulus k and shear modulus μ), and the thermal conductivity λ.

For each property, the dispersion of the results when increasing volume V is reported in Section 5.1. The integral ranges are then identified in Section 5.2. The link between these results and the notion of RVE is postponed to Section 6.

The convention is made that the mean volume of one Voronoï cell is fixed equal to 1 and kept constant. So, a volume V contains $N = V$ Voronoï cells. The results will be given as a function of volume V, which is also equivalent to a number of cells $N = V$. As a result, an increasing volume means an increasing number of grains.

5.1. Study of the average properties

5.1.1. Volume fraction

Consider a microstructure in which there is a given number of Voronoï cells, with a given probability $P_1 = P$ (and $P_2 = 1 - P$), for the random attribution of the two phases 1 and 2. When working with domains of finite size, estimations of P_1 or P_2 are obtained for each realization. So, the obtained volume

fraction found for a given realization of the Voronoï mosaic in a finite volume V will differ from P_1. The number of cells in a volume V is chosen to obey to a Poisson distribution with mean value $N = V$. It means that in a microstructure with N grains, there may not be enough grains to regard it as a representative domain from the point of view of volume fraction of phase 1.

Many realizations of 3D Voronoï mosaic were simulated for increasing volume sizes. The mean volume fraction and its dispersion found for a given volume V (or equivalently mean number of grains N) are given in Fig. 6, as a function of V. It can be seen that the mean volume fraction does not depend on volume size. The mean volume fraction for phase 1 found for small volumes coincides with that found for large ones, provided that a sufficient number of realizations of small volumes are considered. However, the variance decreases with increasing volume size. This study was carried out for the following target mean volume fractions: $P = 50\%, 70\%, 90\%$. The number of realizations considered for each volume size is given in Table 1. This number is chosen so that the obtained mean value and variance do not vary any longer up to a given precision (less than 0.5% here).

As a result, the overall volume fraction of a phase in a heterogeneous material can be determined either by a few number of measurements on large volumes, or by many realizations for small volumes of material. We investigate in the two next subsections whether this reasoning can be extended to physical properties.

5.1.2. Elastic moduli

In this subsection, the Voronoï mosaic is considered as a two-phase linear elastic material. The chosen mechanical properties of the phases are

$$(E_1, \nu_1, k_1, \mu_1) = (2500\ \text{MPa}, 0.3, 2083\ \text{MPa}, 962\ \text{MPa}) \tag{52}$$

$$(E_2, \nu_2, k_2, \mu_2) = (25\ \text{MPa}, 0.49, 417\ \text{MPa}, 8\ \text{MPa}) \tag{53}$$

So the chosen contrast in the Young's modulus is:

$$c = E_1/E_2 = 100 \tag{54}$$

Note that the contrast in shear modulus μ is very high, whereas the contrast in bulk modulus k is weaker. The same microstructures used in the previous study for the volume fraction (in the cases of $P_1 = 70\%$ and $P_2 = 1 - P_1 = 30\%$) are simulated and are introduced in the finite element method for various boundary conditions. The objective of this part is to estimate the apparent mechanical properties (the bulk modulus k^{app} and the shear modulus μ^{app}), as a function of the size of the domain V.

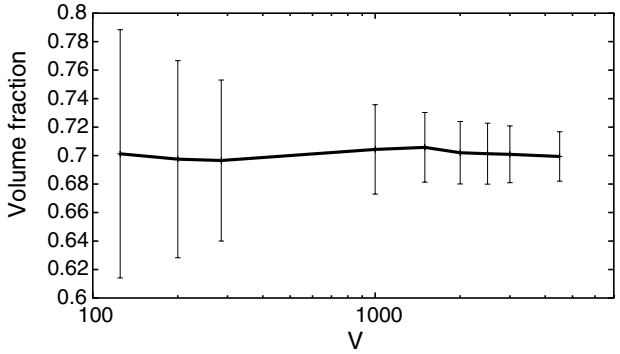

Fig. 6. Mean value and intervals of confidence for volume fraction $P = 70\%$ (results from simulations).

Table 1
Number of realizations n used for all considered domain sizes

Size of the domain (V)	n
6	2500
10	1653
15	1488
37	1238
50	1200
100	1152
125	1020
200	277
285	118
500	35
1000	25
2000	12
2500	14
4000	12
4500	15
8000	13
10000	13
12000	11
14000	10

5.1.2.1. Isotropy of mean apparent moduli. If a small volume element V of a given composite material is considered, it will not a priori exhibit an isotropic behavior. Even if the microstructure is expected to be macroscopically isotropic, the tensor of apparent moduli obtained for a finite domain V is generally not isotropic. We show here however that the mean value of a sufficient number of realizations is isotropic. For that purpose, microstructures of volume V with an average number of 200 Voronoï cells are considered. The anisotropic matrix of the apparent mechanical properties relating mean stress and strain tensors is computed for each realization. Six computations are necessary for each realization to find the 21 apparent elastic coefficients, using here KUBC. The mean value of the matrix of overall mechanical properties is given below. From averaging over 10 different realizations, the obtained matrix is (components in MPa):

$$[C_{10}^{\mathrm{app}}] = \begin{pmatrix} 2034 & 935 & 939 & 5 & 2 & 7 \\ 935 & 1997 & 934 & 1 & 3 & 1 \\ 939 & 934 & 2035 & 1 & 1 & 3 \\ 5 & 1 & 1 & 531 & 1 & 1 \\ 2 & 3 & 1 & 1 & 531 & 1 \\ 7 & 1 & 3 & 1 & 1 & 542 \end{pmatrix} \tag{55}$$

after 30 and 60 different realizations the matrix becomes:

$$[C_{30}^{\mathrm{app}}] = \begin{pmatrix} 2001 & 928 & 928 & 3 & 2 & 7 \\ 928 & 1991 & 927 & 3 & 2 & 0 \\ 928 & 927 & 1995 & 0 & 2 & 4 \\ 3 & 3 & 0 & 526 & 1 & 1 \\ 2 & 2 & 2 & 1 & 525 & 0 \\ 7 & 0 & 4 & 1 & 0 & 528 \end{pmatrix} \tag{56}$$

$$[C_{60}^{\text{app}}] = \begin{pmatrix} 2015 & 935 & 934 & 2 & 1 & 3 \\ 935 & 2013 & 934 & 2 & 1 & 0 \\ 934 & 934 & 2012 & 0 & 1 & 2 \\ 2 & 2 & 0 & 533 & 1 & 0 \\ 1 & 1 & 1 & 1 & 532 & 1 \\ 3 & 0 & 2 & 0 & 1 & 533 \end{pmatrix} \tag{57}$$

The last matrix shows the structure of an isotropic elasticity matrix with bulk and shear moduli equal to: $k^{\text{app}} = 1289$ MPa and $\mu = 533$ MPa.

To estimate these effective values, it is not necessary to compute the whole matrix (six tests on each volume). Instead, for the boundary conditions KUBC for instance, the two deformations $\underset{\sim}{E}_k$ and $\underset{\sim}{E}_\mu$ defined by Eq. (19) can be imposed successively to each realization with volume V. For each realization, two values k^{app} and μ^{app} are obtained (see Eqs. (20) and (21)). The mean values $(\bar{k}^{\text{app}}, \bar{\mu}^{\text{app}})$ over all realizations provide the wanted estimation (associated with the given volume V) of the isotropic effective linear properties. This is the procedure adopted in what follows.

5.1.2.2. Estimation of the apparent elastic moduli. The numerical simulations based on the finite element method are carried out for three different boundary conditions: KUBC, SUBC and the periodic boundary conditions (PERIODIC). The studied volume fraction of hard phase is $P = 70\%$. The number of realizations for each volume is given in Table 1. Fig. 7 gives the obtained mean values and variances of the apparent moduli k^{app} and μ^{app} as a function of the volume size (or equivalently the number of Voronoï cells). It shows that the dispersion of the results decreases when the size of the domain increases for all boundary conditions. As opposite to the case of volume fraction previously studied, the obtained mean values depend on the volume size, but also on the type of boundary conditions. For each modulus, the three values converge towards the same limit for large volumes V, which is the wanted effective modulus. The values k^{eff} and μ^{eff} found for large volume sizes are reported in Table 2 and compared to the Voigt, Reuss and Hashin–Shtrikman bounds. The SC model, also given in Table 2, provides a fair estimate in most cases, except for the volume fraction $P = 50\%$, where it underestimates the moduli. This is due to the fact that the SC model does not properly reproduce the percolation threshold of the mosaic model (which is close to 50%).

It can be noticed that the mean value given by the periodic boundary conditions varies slightly as a function of the size of the domain, as compared to the other boundary conditions. Fig. 7 gives the corresponding confidence intervals $[\overline{Z} - 2D_Z, \overline{Z} + 2D_Z]$, where Z is one of the apparent moduli, $\overline{Z}$ its mean value and D_Z^2 its variance. Finally, an important bias is found in the mean value given by all boundary conditions for small volume sizes, the value being different from the effective one obtained for large specimens. For small volumes, the average moduli obtained by simulations depend on the boundary conditions: KUBC produces results close to the upper Voigt bound, while SUBC gives results close to the lower Reuss bound. This bias is well-known (Huet, 1990; Sab, 1992; Ostoja-Starzewski, 1998). It must be taken into account for the definition of the RVE. The result is that the mean value computed on small specimens cannot represent the effective response for the composite material even using the periodic boundary conditions and a sufficient number of realizations. It appears also that for sufficiently large sizes (here around $V = 15$), the mean value obtained with the periodic boundary conditions practically does not depend on the size of simulations.

5.1.3. Thermal conductivity

Different thermal conductivities are now attributed to the phases of the Voronoï mosaic in order to predict the effective one. The same microstructures used in the study of the RVE for the volume fraction and elasticity ($P = 70\%$), are simulated to determine the apparent thermal properties. The aim of this part is

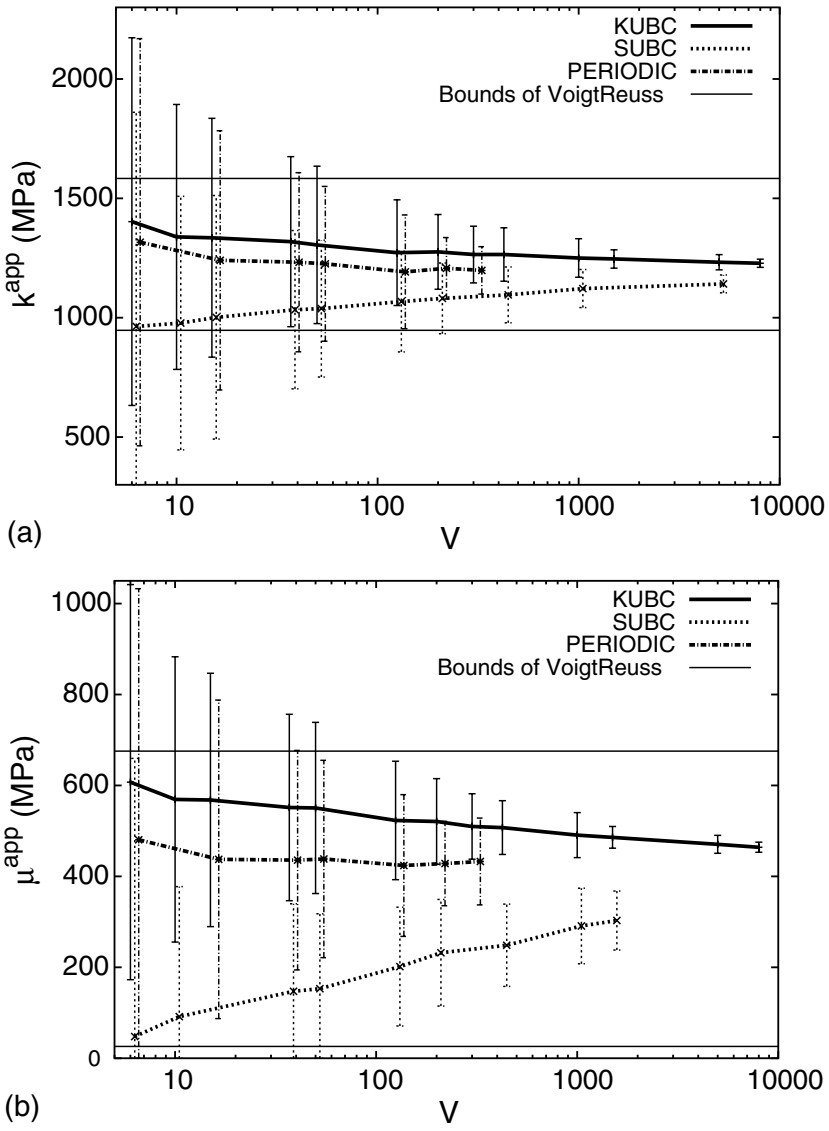

Fig. 7. Mean values and intervals of confidence on the mean value for the bulk modulus k^{app} (a) and shear modulus μ^{app} (b), as a function of domain size ($P_1 = 70\%$). Three different types of boundary conditions are considered. For clarity, the errorbars are slightly shifted around each studied domain size.

to estimate the apparent thermal conductivity λ^{app} of the considered material, as a function of the size of the domain. The chosen thermal conductivities of the phases are

$$(\lambda_1, \lambda_2) = (2.44 \text{ W/mK}, 0.0244 \text{ W/mK}) \tag{58}$$

generating a contrast $c = \lambda_1/\lambda_2 = 100$.

The numerical results are obtained for three boundary conditions: uniform temperature gradient at the boundary (UGT), uniform heat flux at the boundary (UHF) and periodic boundary conditions (PERIODIC). Fig. 8 gives the mean apparent conductivities and associated variances as a function of the domain

Table 2
Values of numerical results, bounds of Voigt–Reuss or Wiener (upper and lower bounds), Hashin–Shtrikman's bounds (HS+, HS−) and SC estimate for elastic and thermal properties studied in this work

Property	Simulation	Upper bound	Lower bound	HS+	HS−	SC
μ ($P = 70\%$, $E_1/E_2 = 100$)	433	676	27	534	39	435
μ ($P = 70\%$, $E_1/E_2 = 1000$)	398	673	3	529	6	404
μ ($P = 50\%$, $E_1/E_2 = 100$)	193	485	17	338	28	147
k ($P = 70\%$, $E_1/E_2 = 100$)	1198	1583	947	1318	955	1194
k ($P = 70\%$, $E_1/E_2 = 1000$)	743	1471	133	1019	135	737
k ($P = 50\%$, $E_1/E_2 = 100$)	833	1250	694	976	699	770
λ ($P = 70\%$, $\lambda_1/\lambda_2 = 100$)	1.346	1.715	0.079	1.498	0.180	1.363

The elastic moduli are given in (MPa), the thermal conductivity in (W/mK).

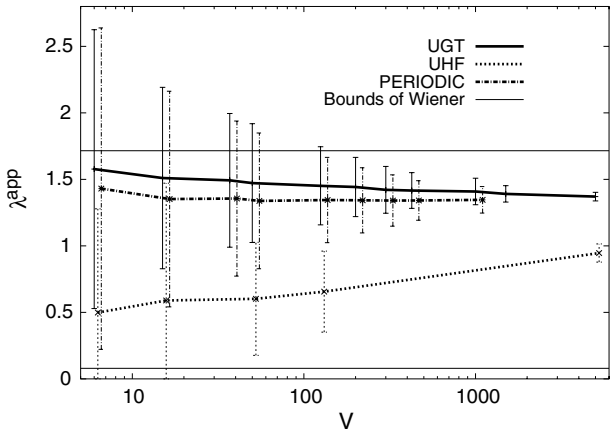

Fig. 8. Dispersion and mean value of the apparent effective thermal conductivity as a function of domain size for different boundary conditions ($c = \lambda_1/\lambda_2 = 100$, $P = 70\%$).

size. It shows that the dispersion of results decreases when the size of the volume increases. The mean value given by the periodic boundary conditions does not vary very much, as compared to the other boundary conditions. The three mean values converge towards the effective thermal conductivity $\lambda^{\text{eff}} = 1.346$ W/mK, which is compared to Wiener's and Hashin–Shtrikman's bounds in Table 2. It can be noticed also that the SC model gives a very good estimate (see Table 2). For small volume elements, the average thermal conductivity obtained by simulations depends on the boundary conditions: UGT gives results close to the upper Wiener bound $\lambda_{\text{Wiener}+}$, and UHF produces results close to the lower Wiener bound $\lambda_{\text{Wiener}-}$:

$$\lambda_{\text{Wiener}+} = P_1\lambda_1 + P_2\lambda_2, \qquad \lambda_{\text{Wiener}-} = \frac{\lambda_1\lambda_2}{P_1\lambda_2 + P_2\lambda_1} \tag{59}$$

The SC model gives the overall thermal conductivity λ^{eff} as the solution of the equation (Beran, 1968):

$$\frac{\lambda_1 - \lambda^{\text{eff}}}{\lambda_1 + 2\lambda^{\text{eff}}}P_1 + \frac{\lambda_2 - \lambda^{\text{eff}}}{\lambda_2 + 2\lambda^{\text{eff}}}P_2 = 0 \tag{60}$$

We have to notice that, as for the apparent elastic moduli, volumes larger than 15 enable us to get an unbiased estimation of λ^{eff} using PERIODIC boundary conditions.

5.2. Fluctuation of apparent properties and determination of the integral ranges

5.2.1. Volume fraction

In this section, we come back to the variance of the volume fraction for the Voronoï mosaic, which is given by Eq. (47). In the three-dimensional case, it becomes:

$$D_P^2(V) = \frac{P(1-P)A_3}{V} \tag{61}$$

where P is the true volume fraction, A_3 is the integral range in 3D for the Voronoï mosaic, and V is the volume of the field containing N cells in average. With the convention that the average volume of one cell is one, the conditions $N = V$ can be substituted in Eq. (61). Fig. 9 is then used to identify A_3 from the simulations presented in Section 5.1.1. Table 3 gives the integral range A_3 estimated from Fig. 9. It is close to the result given by the semi-analytical calculations deduced from (Gilbert, 1962, Eq. (51)), with a larger experimental error for the case $P = 70\%$.

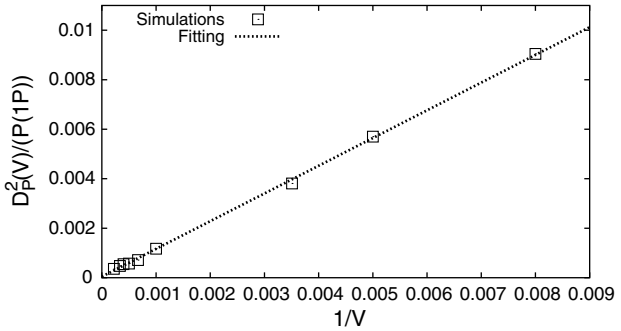

Fig. 9. Fitting of $D_P^2(V)/P(1-P)$ as a function of the inverse of the volume of the field for volume fraction $P = 70\%$. The slope provides the value of the integral range A_3 for the volume fraction.

Table 3
Values of the integral range A_3 and of the coefficient α for different properties and different boundary conditions, identified from the simulation results

Property	Integral range A_3	Coefficient α
$P = 50\%$	1.178 ± 0.023	1
$P = 70\%$	1.111 ± 0.014	1
$P = 90\%$	1.177 ± 0.070	1
k ($P = 70\%$, $E_1/E_2 = 100$) KUBC	2.088 ± 0.045	1.029 ± 0.051
k ($P = 70\%$, $E_1/E_2 = 100$) SUBC	1.267 ± 0.023	0.915 ± 0.044
k ($P = 70\%$, $E_1/E_2 = 100$) PERIODIC	1.020 ± 0.011	0.780 ± 0.037
μ ($P = 70\%$, $E_1/E_2 = 100$) KUBC	1.863 ± 0.046	0.992 ± 0.049
μ ($P = 70\%$, $E_1/E_2 = 100$) SUBC	0.820 ± 0.026	0.735 ± 0.066
μ ($P = 70\%$, $E_1/E_2 = 100$) PERIODIC	1.322 ± 0.009	0.763 ± 0.021
k ($P = 70\%$, $E_1/E_2 = 1000$) PERIODIC	1.650 ± 0.017	0.900 ± 0.038
μ ($P = 70\%$, $E_1/E_2 = 1000$) PERIODIC	2.097 ± 0.015	0.862 ± 0.023
k ($P = 50\%$, $E_1/E_2 = 100$) PERIODIC	1.589 ± 0.050	0.875 ± 0.010
μ ($P = 50\%$, $E_1/E_2 = 100$) PERIODIC	1.637 ± 0.016	1.009 ± 0.036
λ ($P = 70\%$, $\lambda_1/\lambda_2 = 100$) UGT	2.335 ± 0.258	1.070 ± 0.021
λ ($P = 70\%$, $\lambda_1/\lambda_2 = 100$) UHF	2.036 ± 0.407	0.978 ± 0.031
λ ($P = 70\%$, $\lambda_1/\lambda_2 = 100$) PERIODIC	2.619 ± 0.200	1.033 ± 0.018

5.2.2. Elastic moduli

As recalled in Section 3.2, the effective properties are defined from spatial averages of fields $Z(x)$ over a volume V. We will have to consider now fluctuations of the average values over different realizations of the random composite material inside the volume V. In geostatistics, it is well known that for an ergodic stationary random function $Z(x)$, one can compute the variance $D_Z^2(V)$ of its average value $\overline{Z}(V)$ over the volume V (Matheron, 1971; Lantuéjoul, 1991):

$$D_Z^2(V) = D_Z^2 \frac{A_3}{V} \tag{62}$$

where D_Z^2 is the point variance of $Z(x)$ and A_3 is the integral range of the random function $Z(x)$. This is a generalization to any random function $Z(x)$ of the notion introduced for the volume fraction in Section 3.2.

The scaling law (62) is valid for an additive combination of the variable Z over the region of interest V, when its size is such that $V > A_3$ and when A_3 is finite. For an infinite integral range, V can be replaced in many cases by V^α (with $\alpha \neq 1$) in relation (62) (Lantuéjoul, 1991).

As the composition of elastic moduli in the change of scale is not additive in general, relation (62) cannot be applied. Instead we propose to test a power law (called "model" in what follows) according to the relation:

$$D_Z^2(V) = D_Z^2 \left(\frac{A_3}{V} \right)^\alpha \tag{63}$$

A similar relation was proposed and tested by Cailletaud et al. (1994). In the case of a two-phase material with elastic property Z_1 for phase 1 and Z_2 for phase 2, the point variance D_Z^2 of the random variable Z is given by:

$$D_Z^2 = P(1-P)(Z_1 - Z_2)^2 \tag{64}$$

The relation (63) becomes:

$$D_Z^2(V) = P(1-P)(Z_1 - Z_2)^2 \left(\frac{A_3}{V} \right)^\alpha \tag{65}$$

For the elastic properties (52) and (53) chosen in this work, Eq. (64) yields: $D_k^2 = 583,329$ (MPa)^2 and $D_\mu^2 = 190,784$ (MPa)^2. Eq. (63) can be written as:

$$\log(D_Z^2(V)) = -\alpha \log(V) + (\log(D_Z^2) + \alpha \log(A_3)) \tag{66}$$

Our data were fit to relation (66) for the elastic moduli k^{app} and μ^{app} and different boundary conditions. The found parameters A_3 and α are given in Table 3. The quality of the model can be seen in Fig. 10, where the variances of simulated results and the model are compared for all considered boundary conditions. The power law is especially well-suited for PERIODIC boundary conditions.

It is clear, from the coefficients given in Table 3, that the proposed scaling law in relation (63) can be accepted for our simulations. The value of the integral range depends on the boundary conditions. It is of the order of the integral range of the volume fraction for periodic and SUBC conditions. The largest integral range of the elastic moduli is found for the periodic boundary conditions and the coefficient α is close to (but generally smaller than) 1. It means that the variance decreases more slowly with the volume than the variance of the volume fraction in all cases. Note that the value of the coefficient α found by Cailletaud et al. (1994) is also close to 1 for a 2D random mosaic. Another conclusion is that larger domains (or more realizations) must be used to estimate the elastic moduli with a given precision, for SUBC than for KUBC boundary conditions. This will be illustrated later.

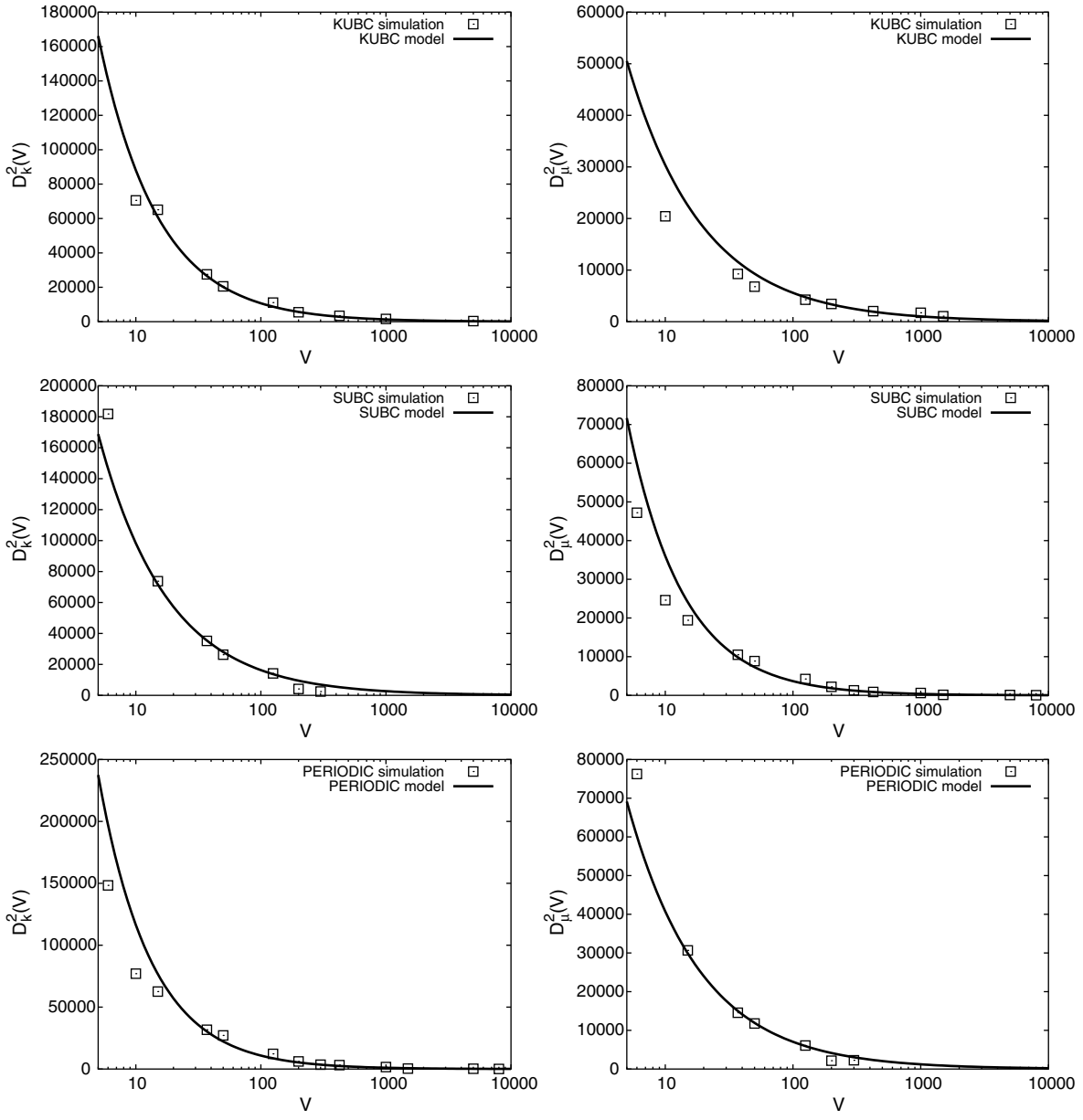

Fig. 10. Variances of the apparent elastic moduli k^{app} and μ^{app} for different boundary conditions: simulations and model.

5.3. Effect of the volume fraction and contrast on the integral ranges

The apparent properties and integral ranges obtained for elasticity depend on the volume fraction of phases. A second volume fraction $P_1 = P_2 = P = 50\%$ is investigated here in addition to the previous one $P_1 = 70\%$. These microstructures are also simulated and introduced in the finite element software with the same mechanical properties, given by (52) and (53). The objective is to study the effect of the

volume fraction on the integral ranges of the apparent bulk and shear moduli k^{app} and μ^{app}. The numerical simulations using the finite element method were performed in this case only for the periodic boundary conditions. The mean values and variances are given in Fig. 11 as a function of the domain size. The mean value varies slowly as a function of the size of the domain. Again, an important bias in the mean value for small sizes of specimens is observed. For domain sizes larger than $V = 37$, the mean values are almost constant, and coincide with the effective properties. This size is larger than for $P = 70\%$ (where $V \simeq 15$ according to Fig. 7). The values of the integral ranges and of the coefficient α, obtained by identification of the power law model (Eq. (63)) from the numerical results, are given in Table 3. It can be noticed that the values of the integral ranges and those of the coefficient α obtained in the case of $P = 50\%$ are larger than those obtained in the case of $P = 70\%$, for a given contrast of properties. The coefficients α remains close to 1 for all investigated volume fractions.

Another important source of fluctuations of apparent moduli of finite domains is the contrast of properties $c = E_1/E_2$. So far, only the case $c = 100$ has been investigated. Let us now consider a contrast $c = 1000$ (E_1 keeping its value 2500 MPa), for $P = 70\%$. The objective is to study the effect of the contrast on the integral ranges of the effective elastic properties. The numerical simulations are performed for periodic boundary conditions. Results are shown in Fig. 12. A bias in the mean value in this case is observed when $V < 15$ grains (as in the case of a contrast $c = 100$). The values of the integral ranges and of the coefficient α, obtained by fitting the numerical results, using the model (Eq. (63)), are given in Table 3. The values of the integral ranges obtained in the case of ($c = 1000$, $P = 70\%$) are much larger than those obtained in the case of ($c = 100$, $P = 70\%$). The values of the coefficient α remain close to 1.

5.3.1. Thermal conductivity

The power law model proposed in the case of elastic properties (Eq. (63)) can be used also for apparent thermal properties. The point variance D_λ^2 is:

$$D_\lambda^2 = P(1-P)(\lambda_1 - \lambda_2)^2 = 1.2253\ (\mathrm{W/mK})^2 \tag{67}$$

The values of the integral ranges and of the coefficient α identified from the simulations are given in Table 3 for different boundary conditions. They are found to depend on the type of boundary conditions. The largest integral range for the thermal conductivity is obtained for the periodic boundary conditions and the

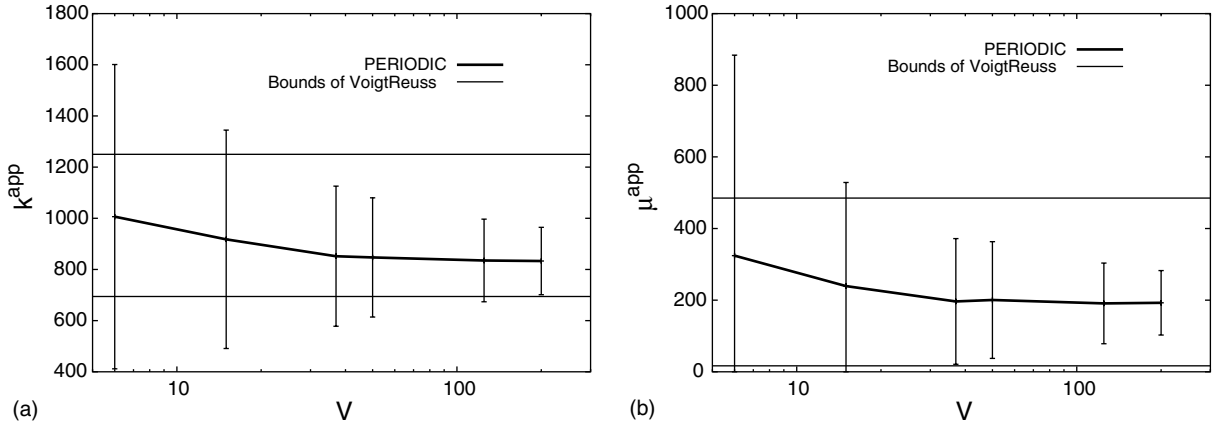

Fig. 11. Dispersion and mean value of the apparent elastic properties as a function of the domain size for periodic boundary conditions in the case of ($c = 100$, $P = 50\%$): (a) evolution of k and (b) evolution of μ.

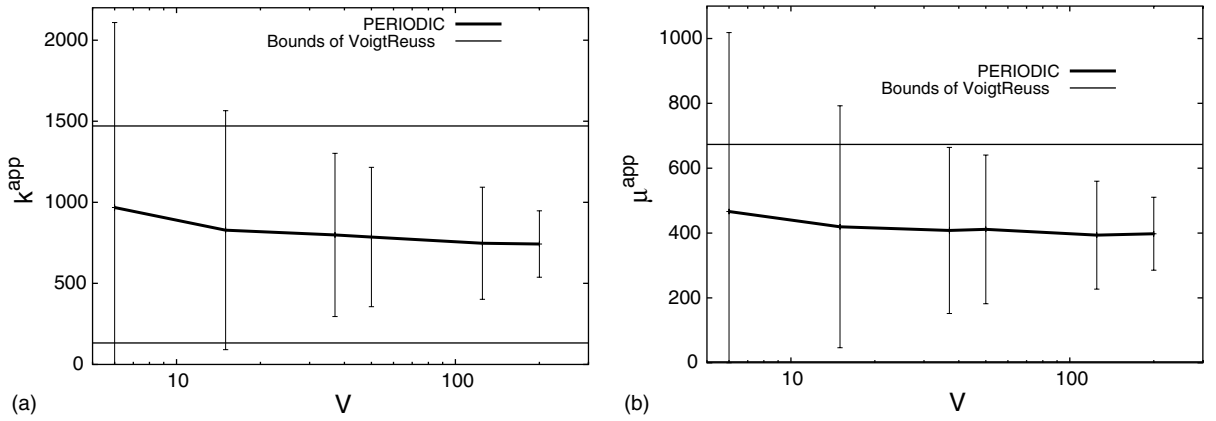

Fig. 12. Dispersion and mean value of the apparent elastic properties as a function of the domain size for periodic boundary conditions in the case ($c = 1000$, $P = 70\%$): (a) evolution of k^{app} and (b) evolution of μ^{app}.

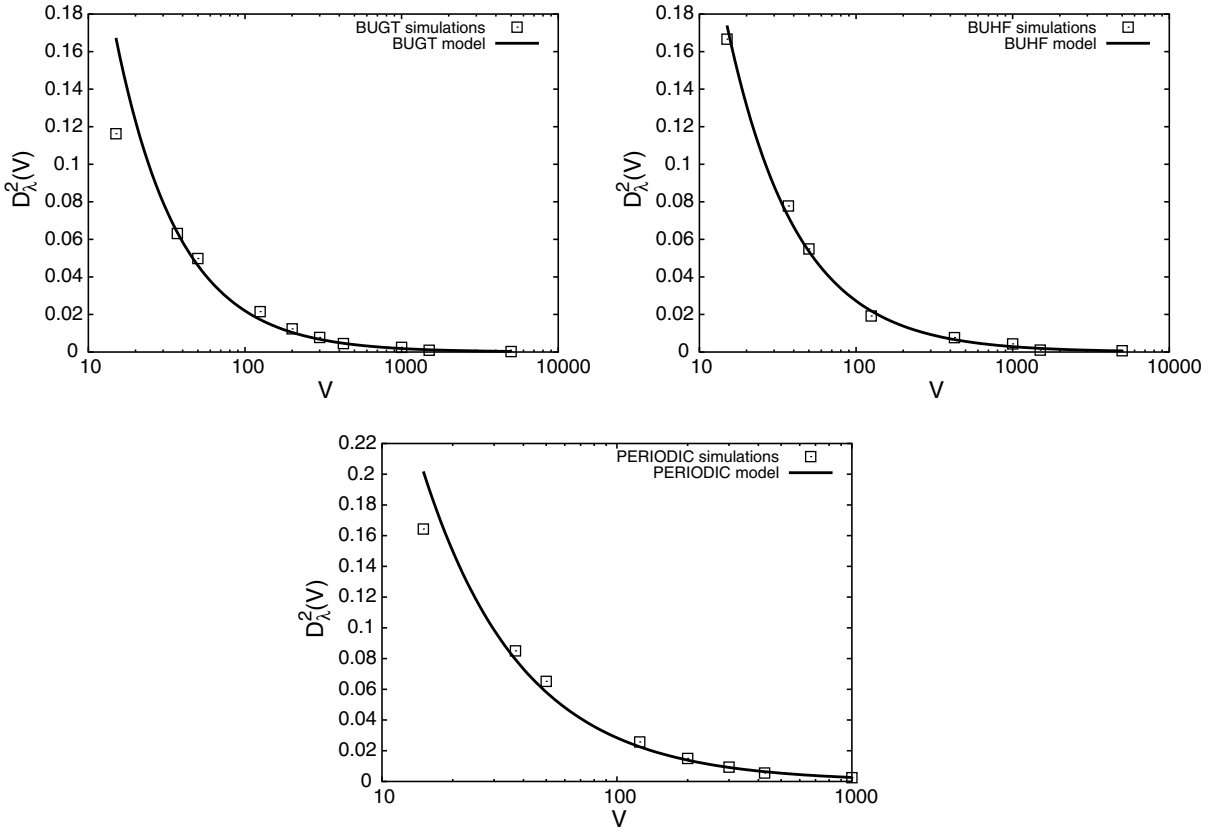

Fig. 13. Variances of apparent thermal conductivity λ^{app} for different boundary conditions $P = 70\%$.

coefficient α is close to 1. These parameters are larger than for the case of elasticity. Fig. 13 shows the quality of the model. The power law is especially well-suited for periodic boundary conditions.

6. Determination of the size of the RVE

When considering a material as a realization of a random set or of a random function, we will show that the idea that there exists one single possible minimal RVE size must be abandoned. Instead, the size of a RVE can be defined for a given physical property, a given contrast and, above all, a given precision in the estimation of the effective properties and given number of realizations that one is ready to generate. This is explicited later for the three situations encountered in the previous sections.

The size of a RVE for an estimated property Z can be related directly to the precision of the mean value of the results of different realizations for each domain size. So, theoretically, if the domain V is a RVE for the property Z, the dispersion must vanish. In practice one must determine the size of the RVE for a *given error* ε. In the theory of samples, the absolute error on the mean value obtained with n independent realizations of volume V is deduced from the interval of confidence by:

$$\varepsilon_{\text{abs}} = \frac{2D_Z(V)}{\sqrt{n}} \tag{68}$$

Hence the relative error $\varepsilon_{\text{rela}}$ is:

$$\varepsilon_{\text{rela}} = \frac{\varepsilon_{\text{abs}}}{Z} = \frac{2D_Z(V)}{Z\sqrt{n}} \tag{69}$$

The size of the RVE can now be defined as the volume for which for instance $n = 1$ realization is necessary to estimate the mean property Z with a relative error $\varepsilon_{\text{rela}} = 1\%$, provided we know the function $D_Z(V)$. Alternatively, we can decide to operate on smaller volumes (provided no bias is introduced), and consider n realizations to obtain the same relative error. Eq. (69) gives:

$$n = \frac{4D_Z^2(V)}{Z^2\varepsilon_{\text{rela}}^2} \tag{70}$$

6.1. Volume fraction

In the case of the volume fraction, the exact mean value $P^{\text{eff}} = P$ is known. The relative error is given as a function of the sampled volume V by:

$$\varepsilon_{\text{rela}}(V) = \frac{2D_P(V)}{P} = 2\sqrt{\frac{(1-P)A_3}{VP}} \tag{71}$$

which corresponds to the application of Eq. (68) for $n = 1$. This is illustrated in Fig. 14 in the case of a volume fraction $P = 70\%$. Using Eq. (71), the minimum domain size that is necessary to reach a given precision are shown, for three different volume fractions, in Table 4.

The size of a RVE for the estimated volume fraction can be related directly to the precision of the mean value of the results of different realizations for each domain size. Fig. 14 shows three examples of this measurement: one obtains $V_{5\%}^{\text{RVE}} = 800$, $V_{2\%}^{\text{RVE}} = 5050$ and $V_{1\%}^{\text{RVE}} = 20,000$ for the relative precision $\varepsilon_{\text{rela}} = 5\%$, $\varepsilon_{\text{rela}} = 2\%$ and $\varepsilon_{\text{rela}} = 1\%$ of the mean value of the volume fraction, respectively. The size of the RVE can also be defined as the volume for which for instance $n = 10$ realizations are necessary to estimate the mean property with a confidence $\varepsilon_{\text{rela}} = 1\%$. Eq. (71) gives:

$$V = \frac{4(1-P)A_3}{nP\varepsilon_{\text{rela}}^2} \tag{72}$$

For $P = 70\%$ one finds $V^{\text{RVE}} = 2000$. Conversely, the same equation also shows that one must use about $n = 1350$ realizations to find the mean value with an error $\varepsilon_{\text{rela}} = 1\%$ for a fixed $V^{\text{RVE}} = 15$.

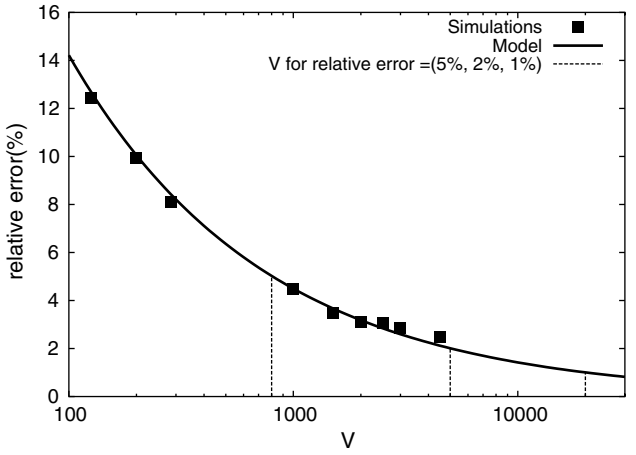

Fig. 14. Relative precision $\varepsilon_{\text{rela}}$ for volume fraction $P = 70\%$ and $n = 1$ realization: It decreases when the size of the domain increases.

Table 4
RVE size for a given relative precision $\varepsilon_{\text{rela}}$ and $n = 1$ realization of the estimated volume fraction, for three different volume fractions

Volume fraction P	1%	2%	5%	10%
50%	47,000	11,790	1880	470
70%	20,000	5050	800	200
90%	5240	1300	210	52

6.2. Elastic moduli

In the case of effective elastic moduli, the exact mean value and variance for a given domain size are a priori unknown. Using Eq. (63), the absolute error on the mean value can be evaluated as:

$$2D_Z(V) = 2D_Z\sqrt{\left(\frac{A_3}{V}\right)^{\alpha}} \tag{73}$$

where Z stands here for k^{app} or μ^{app}. The absolute error can be deduced from Fig. 10 that shows the power law model and the variances of simulations as a function of domain size, for different boundary conditions.

The first important remark is that for the same absolute error, the periodic boundary conditions require the largest domain size, compared to KUBC and SUBC for k and μ. This is due to higher fluctuations of apparent properties obtained with these conditions. The KUBC require a smaller domain size than the SUBC for the same absolute error.

Using Eq. (68) in the case of the elastic moduli k^{app} and μ^{app}, the absolute error for the mean value is obtained with a sample of n realizations, Z standing for k^{app} or μ^{app}. Hence the number of realizations n necessary for the estimation of the property with a given absolute error ε_{abs} and a volume V is:

$$n(V) = \frac{4}{\varepsilon_{\text{abs}}^2} D_Z^2 \left(\frac{A_3}{V}\right)^{\alpha} \tag{74}$$

One must insist on the fact that the absolute error corresponds to the estimation of the mean apparent moduli which have been found to depend in general on the domain size and do not necessarily coincide with the wanted effective property, especially for small domain sizes. This corresponds to a bias of the

estimation. This bias is bounded by the difference of the estimations obtained using KUBC and SUBC, since these boundary conditions can be shown to provide bounds of the the effective properties (Huet, 1990; Hazanov and Huet, 1994). From the available results of Fig. 7, the smallest domain size for which the bias can be neglected is $V = 15$ grains for k^{app} and μ^{app} in the case of periodic boundary conditions. For the conditions KUBC and SUBC, volumes larger than 1000 are necessary to obtained unbiased mean values, i.e. mean apparent moduli that almost coincide with the wanted effective ones.

Using Eq. (69), and for a volume V providing unbiased moduli, we deduce the relative precision of the effective property Z^{eff} (namely the effective bulk modulus k^{eff} or the effective shear modulus μ^{eff}). Hence, the number n of realizations that must be considered is deduced from Eqs. (70) and (73). This is illustrated in Fig. 15 for $\varepsilon_{\text{rela}} = 1\%$. For a given precision, the number of realizations decreases when the domain size increases. The periodic boundary conditions require the largest number of realizations, compared with other boundary conditions. Let us give two explicit examples of the use of Eq. (70) for two unbiased volumes and periodic boundary conditions: $V = 50$ and $V = 125$. The minimal numbers n of realizations to obtain the overall bulk modulus k^{eff} and shear modulus μ^{eff}, for a given precision $\varepsilon_{\text{rela}}$, are given in Table 5.

Conversely, the minimum size of the RVE can be determined for a given $\varepsilon_{\text{rela}}$ and a given number $n = 10$ of realizations. The results are shown on Fig. 15. When $\varepsilon_{\text{rela}} = 1\%$, it can be seen that one must take about $V^{\text{RVE}} = 13,340$ (from the result given by the periodic boundary conditions) for k^{app} and $V^{\text{RVE}} = 71,253$ for μ^{app}. Using such sizes in a finite element code is rather prohibitive. One would prefer smaller volumes. This requires however a sufficient number of realizations. By comparison between these results and those for volume fraction in Table 4, it turns out that larger volumes are required to estimate the elastic moduli than

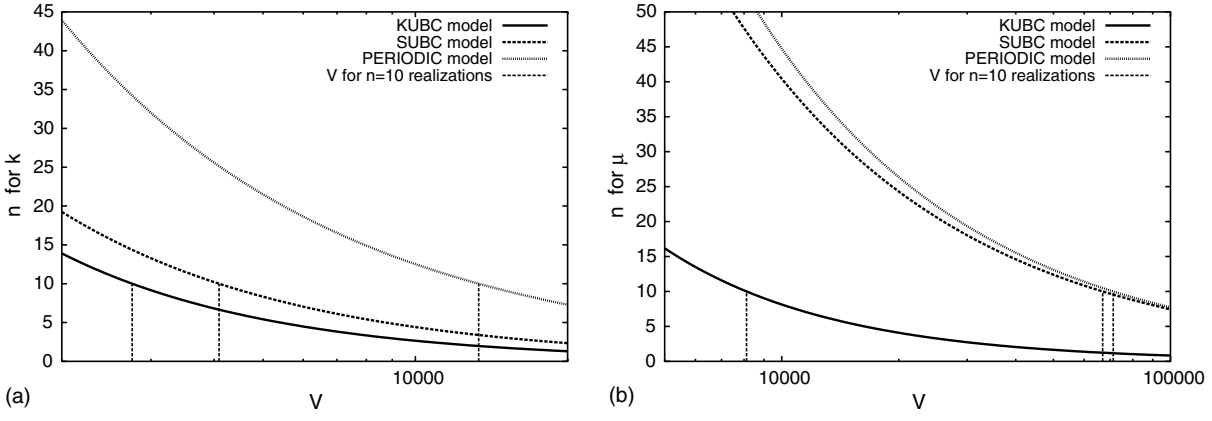

Fig. 15. Number of realizations as a function of the domain size for a given relative error $\varepsilon_{\text{rela}} = 1\%$: (a) case of k^{app} and (b) case of μ^{app}.

Table 5
Minimal number of realizations necessary to estimate the effective elastic moduli and thermal conductivity with given relative precision, for given volumes $V = 50$, 125 (for periodic boundary conditions, $P = 70\%$, $c = 100$)

Relative precision	$\varepsilon_{\text{rela}} = 1\%$	$\varepsilon_{\text{rela}} = 2\%$	$\varepsilon_{\text{rela}} = 5\%$	$\varepsilon_{\text{rela}} = 10\%$
Bulk modulus ($V = 50$)	700	175	28	7
Shear modulus ($V = 50$)	2500	625	100	25
Bulk modulus ($V = 125$)	400	100	16	4
Shear modulus ($V = 125$)	1300	325	52	13
Thermal conductivity ($V = 50$)	1950	490	80	20
Thermal conductivity ($V = 125$)	765	190	30	8

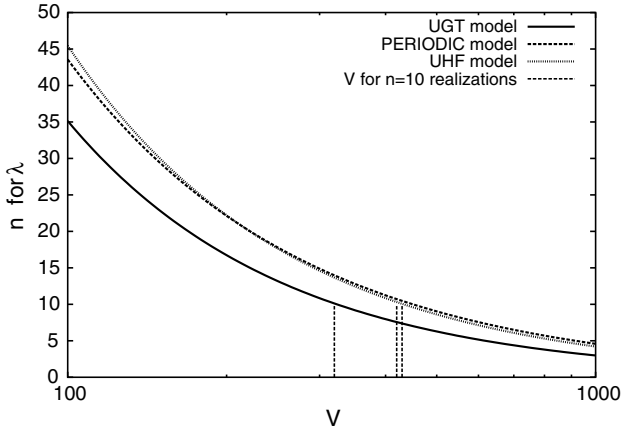

Fig. 16. Number of realizations as a function of the domain size, necessary to obtain an absolute precision $\varepsilon_{abs} = 0.05$ W/mK on the mean value of apparent thermal conductivity $P = 70\%$.

to measure the volume fraction with the same precision (over three times more). In the present study, the shear modulus requires a larger number of realizations than the bulk modulus, for a given precision.

6.3. Thermal conductivity

Similarly to the case of elastic properties, the absolute error on the mean value of apparent conductivity is given by relation (73). For the same absolute error on the mean value, the periodic boundary conditions require the largest domain size compared to the other boundary conditions. The UGT conditions give a smaller domain size than the uniform heat flux for the same absolute error. The number of realizations n for a given relative error ε_{rela} on the effective conductivity λ^{eff} is deduced from Eq. (69). It is illustrated in Fig. 16 for $\varepsilon_{rela} = 1\%$. For a given precision, the required number of realizations decreases when the volume increases. The periodic boundary conditions (PERIODIC) require the largest number of realizations, as compared to other boundary conditions. The size of the RVE, considered for instance as the volume requiring only $n = 10$ realizations, for $\varepsilon_{rela} = 1\%$ is about $V = 5504$ (periodic boundary conditions).

One must again insist on the fact that the mean value of the apparent conductivity depends on the domain size. Volumes larger than $V = 100$ are necessary to obtain a mean apparent conductivity which is not too far from the effective one λ^{eff}, for the conditions UGT and UHF. The smallest domain size giving an unbiased mean value of apparent conductivity is about 10 for PERIODIC conditions. Using Eq. (70) in the case of the effective thermal conductivity, the minimal numbers n of realizations to evaluate the effective thermal conductivity with a given precision ε_{rela}, are given in Table 5 for the fixed sizes $V_1 = 50$ grains and $V_2 = 125$ grains.

7. Conclusions

The effective linear properties of random composites can be determined not only by numerical simulations on large volume elements of heterogeneous material, but also as mean values of apparent properties of rather small volumes, providing that a sufficient number of realizations is considered. This is very important, since computations on large volumes are usually prohibitive. This corresponds also to an enlarged definition of RVE. Its size V^{RVE} must be considered as a function of five parameters: the physical property

Z, the contrast of properties c, the volume fractions of components, the wanted relative precision $\varepsilon_{\text{rela}}$ for the estimation of the effective property and the number n of realizations of the microstructure associated with computations that one is ready to carry out. It depends also *in fine* on the special morphology of distribution of phases. Conversely, one can also choose a volume V^{RVE} allowing as many numerical simulations as necessary. The proposed methodology gives then the number of realizations that are necessary to reach a given precision $\varepsilon_{\text{rela}}$ (see for instance Eq. (74)).

However, the chosen volume V^{RVE} cannot be taken as small as one may wish, because there exists in general a bias in the estimation of the effective properties. This bias is due to the type of boundary conditions. The mean apparent properties computed on finite size domains do not coincide with the effective ones if the domain size is too small. In the case of linear elasticity for instance, KUBC overestimate the effective properties, whereas SUBC underestimate them. For both thermal conductivity and elasticity, the bias introduced by the periodic boundary conditions is found to be much smaller than for the other boundary conditions. In the case of Voronoï mosaics considered in this work, for domain sizes larger than $V = 15$ (respectively $V = 37$) for volume fraction $P_1 = 70\%$ (respectively $P_1 = 50\%$), the mean apparent property do not differ significantly from the effective one. However the dispersion of apparent properties obtained by periodicity conditions is always found to be larger than for the other types of boundary conditions. This means that more realizations are necessary (about 1700 for elasticity with $V = 15$, $\varepsilon_{\text{rela}} = 5\%$, $P_1 = 70\%$, $c = 100$).

For the determination of RVE sizes of a given microstructure, the proposed methodology can be summarized as follows:

- generate different realizations of the microstructure for 4–5 different volume sizes V;
- submit each microstructure to loading with for instance periodic boundary conditions and record the obtained apparent properties;
- compute mean value and variance of apparent property for the considered volume sizes; check that the number of realizations was sufficient for each volume (apply the sampling rule (68));
- identify the integral range A_3 and power α in model (73);
- set the wanted precision for the estimation of effective property $\varepsilon_{\text{rela}}$ and a number of realizations n; use the model to deduce the final size V^{RVE}.

The notion of integral range plays the central rôle in the method. For additive properties (like volume fraction or mass density), it is simply related to the variance and domain size and does not depend on the effective property itself but only on the morphology. For more complex physical properties like elasticity and thermal conductivity, a power law model was proposed and identified. The generalized integral range A_3 is found to depend on the volume fraction, the contrast in properties, and the type of boundary conditions. The model seems to fit better to the data in the case of periodic boundary conditions. This can be related to the fact that the observed bias in the estimation of effective properties is less pronounced in the case of periodic boundary conditions.

The case of 3D Voronoï mosaics was studied in details, as an example of random microstructures. This model is relevant for polycrystals but also for two-phase materials in which both phases percolate. The fluctuations of apparent moduli on small domains can be attributed to the percolation level of the hard phase for the considered realization. This could explain the larger values found for the integral range A_3 found for the volume fraction $P_1 = 50\%$ than for $P_1 = 70\%$. This is synonymous of a larger dispersion of apparent moduli and finally to larger RVE sizes. Similarly, the increase in the contrast of properties leads to an increase of the integral range and of the RVE size. The RVE sizes found for different properties can be compared: the minimal domain size for a relative precision of 1% in the estimated property, $n = 10$ realizations and for $P_1 = 70\%$, $c = 100$ are $V = 2000$, 5504, 13,340, 71,253 for effective volume fraction, thermal conductivity, bulk modulus and shear modulus, respectively, in increasing order of volume size. These

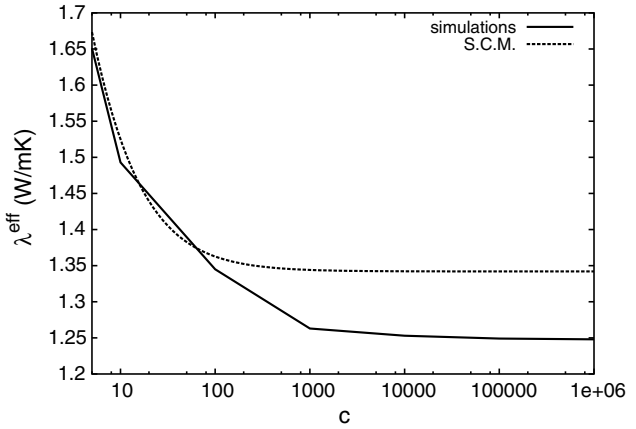

Fig. 17. Effective thermal conductivity of Voronoï mosaics as function of the contrast of properties c (the thermal conductivity $\lambda_1 = 2.44$ W/mK is kept constant, $P_1 = 70\%$): comparison with the SC estimate. The numerical estimation of the effective conductivity is obtained by finite element simulations with periodic boundary conditions on a volume $V = 125$ and $n = 1020$ realizations for each value of c. The mean value is plotted.

results depend on the specific values chosen for the material parameters of the components in the simulation, and do not have a general value. Note that the SC estimate is often advocated to be a good model for polycrystalline microstructures. Indeed, a rather good agreement between the found effective properties of two-phase Voronoï mosaics and the SC model can be seen in Table 2. This is however not the exact solution (for elasticity nor thermal conductivity) and the difference between numerical simulations and the SC estimate is found to increase with the contrast of properties, as can be seen in Fig. 17 for thermal properties. Another example of bicontinuous microstructure that is not described properly by the SC scheme can be found in Roberts and Garboczi (1999), where computational homogenization methods are also used.

The procedure must now be applied to other microstructures and random models. It can also be applied to real three-dimensional images of heterogeneous materials obtained by tomography or confocal microscopy for instance (Forest et al., 2002). Good agreement has been obtained between experimental results and the numerical estimation of the effective elastic and thermal properties of a two-phase material from food industry (Kanit et al., in preparation). In particular, it is shown in this forthcoming paper that the methodology can be used to assess the representativity of available 3D images. In such cases, it may be necessary to estimate the properties using images smaller than the size of the deterministic RVE. On the other hand, the advantage of the method is that it is applicable also to nonlinear constitutive behaviours of the components (viscoplasticity, elastoplasticity). An increased dependence of the integral range on the contrast of properties may be expected in the nonlinear case, as a result of a higher heterogeneity of the fields.

References

Barbe, F., Decker, L., Jeulin, D., Cailletaud, G., 2001a. Intergranular and intragranular behavior of polycrystalline aggregates. Part 1: FE model. Int. J. Plasticity 17, 513–536.

Barbe, F., Forest, S., Cailletaud, G., 2001b. Intergranular and intragranular behavior of polycrystalline aggregates. Part 2: Results. Int. J. Plasticity 17, 537–563.

Beran, M.J., 1968. Statistical Continuum Theories. John Wiley, New York.

Besson, J., Cailletaud, G., Chaboche, J.L., Forest, S., 2001. Mécanique non linéaire des matériaux. Hermès Science.
Bornert, M., Bretheau, T., Gilormini, P., 2001. Homogénéisation en mécanique des matériaux. Hermès.
Cailletaud, G., Jeulin, D., Rolland, P., 1994. Size effect on elastic properties of random composites. Engng. Computat. 11, 99–110.
Colworth, U.R., 2000. Unilever Laboratory Progress Report.
Coster, M., Chermant, J.L., 1989. Précis d'Analyse d'Images. Presses du CNRS.
Decker, L., Jeulin, D., 2000. Simulation 3D de matériaux aléatoires polycristallins. La Revue de Métallurgie-CIT/Science et Génie des Matériaux, 271–275.
Drugan, W.J., Willis, J.R., 1996. A micromechanics-based nonlocal constitutive equations and estimates of representative volume element size for elastic composites. J. Mech. Phys. Solids 44, 497–524.
Fahrat, C., Roux, F.X., 1994. Implicit parallel processing in structural mechanics. Comput. Mech. Adv. 2, 47–72.
Feyel, F., 1998. Application du calcul parallèle aux modèles à grand nombre de variables internes, Thèse de Doctorat. Ecole des Mines de Paris.
Feyel, F., Cailletaud, G., Kruch, S., Roux, F.X., 1997. Application du calcul parallèle aux modèles à grand nombre de variables internes. Colloque national en calcul de structures, May 20–23, Giens, France, pp. 309–314.
Forest, S., Barbe, F., Cailletaud, G., 2000. Cosserat modelling of size effects in the mechanical behavior of polycrystals and multi-phase materials. Int. J. Solids Struct. 37, 7105–7126.
Forest, S., Cailletaud, G., Jeulin, D., Feyel, F., Galliet, I., Mounoury, V., Quilici, S., 2002. Introduction au calcul de microstructures. Mécanique et Industries 3, 439–456.
Ghosh, S., Moorthey, S., 1995. Elastic–plastic analysis of arbitrary heterogeneous materials with the Voronoi Cell finite element method. Comput. Methods Appl. Mech. Engng. 121, 373–409.
Gilbert, E.N., 1962. Random subdivisions of space into crystals. Ann. Math. Stat. 33, 958–972.
Gusev, A.A., 1997. Representative volume element size for elastic composites: a numerical study. J. Mech. Phys. Solids 45, 1449–1459.
Hashin, Z., Shtrikman, S., 1963. A variational approach to the theory of elastic behavior of multiphase materials. J. Mech. Phys. Solids 11, 127–140.
Hazanov, S., Huet, C., 1994. Order relationships for boundary conditions effect in heterogeneous bodies smaller than the representative volume. J. Mech. Phys. Solids 42, 1995–2011.
Hershey, A.V., 1954. The elasticity of an isotropic aggregate of anisotropic cubic crystals. J. Appl. Mech. 21, 236–240.
Huet, C., 1990. Application of variational concepts to size effects in elastic heterogeneous bodies. J. Mech. Phys. Solids 38, 813–841.
Jeulin, D., 1981. Mathematical morphology and multiphase materials. In: Proceedings of 3rd European Symposium of Stereology, vol. 3, suppl. 1. Streol. Iugosl., pp. 265–286.
Jeulin, D., 2001. Caractérisation Morphologique et Modèles de Structures Aléatoires, Extrait de: Homogénéisation en mécanique des matériaux (tome1). Hermès, France.
Jeulin, D., Ostoja-Starzewski, M., 2001. Mechanics of Random and Multiscale Microstructures, vol. 430. CISM Lecture Notes, Springer-Verlag.
Kanit, T., Forest, S., Mounoury, V., Jeulin, D., in preparation. Large-scale computations of two-phase microstructures from confocal 3D images: elastic and thermal properties.
Kröner, E., 1958. Berechnung der elastischen Konstanten des Vielkristalls aus des Konstanten des Einkristalls. Z. Physik 151, 504–518.
Kröner, E., 1980. Linear properties of random media—the systematic theory. Comportements rhéologiques et structure des matériaux-CR 15ème Coll. GFR. Paris.
Lantuéjoul, C., 1991. Ergodicity and integral range. J. Microsc. 161, 387–403.
Lippmann, N., Steinkopf, T., Schmauder, S., Gumbsch, P., 1997. 3d-finite-element-modelling of microstructures with the method of multiphase elements. Comput. Mater. Sci. 9, 28–35.
Matheron, G., 1971. The Theory of Regionalized Variables and its Applications. Paris School of Mines publications.
Matheron, G., 1975. Random Sets and Integral Geometry. John Wiley, New York.
Matheron, G., 1989. Estimating and Choosing. Springer-Verlag, Berlin.
Meille, S., Garboczi, E., 2001. Linear elastic properties of 2-d and 3-d models of porous materials made from elongated objects. Mod. Sim. Mater. Sci. Engng. 9, 1–20.
Miller, M., 1969. Bounds for the effective electrical, thermal and magnetic properties of heterogeneous materials. J. Math. Phys. 10, 1988–2004.
Milton, G., 1982. Bounds on the elastic and transport properties of two component composites. J. Mech. Phys. Solids 30, 177–191.
Milton, G., 1985. The coherent potential approximation is a realizable effective medium scheme. Commun. Math. Phys. 99, 453–500.
Nemat-Nasser, S., Hori, M., 1993. Micromechanics: Overall Properties of Heterogenous Materials. North Holland, Amsterdam.
Ostoja-Starzewski, M., 1998. Random field models of heterogeneous materials. Int. J. Solids Struct. 35 (19), 2429–2455.
Ponte Castañeda, P., Suquet, P., 1987. Nonlinear composites. Adv. Appl. Mech., 34.
Povirk, G.L., 1994. Incorporation of microstructural information into models of two-phase materials. Acta Metall. Mater. 43, 3199–3206.

Roberts, A., Garboczi, E., 1999. Elastic properties of a tungste-silver composite by reconstruction and computation. J. Mech. Phys. Solids 47, 2029–2055.

Roberts, A., Garboczi, E., 2000. Elastic properties of model porous ceramics. J. Am. Ceram. Soc. 83 (12), 3041–3048.

Roberts, A., Garboczi, E., 2001. Elastic moduli of model random three-dimensional closed-cell cellular solids. Acta Mater. 49, 189–197.

Sab, K., 1992. On the homogenization and the simulation of random materials. Eur. J. Mech. Solids 11, 585–607.

Sanchez-Palencia, E., Zaoui, A., 1987. Homogenization techniques for composite media. Lecture Notes in Physics No. 272, Springer-Verlag, Berlin.

Serra, J., 1982. Image Analysis and Mathematical Morphology. Academic Press.

Suquet, P., 1997. Continuum micromechanics. CISM Courses and Lectures No. 377, Springer-Verlag, Berlin.

Terada, K., Ito, T., Kikuchi, N., 1998. Characterization of the mechanical behaviors of solid-fluid mixture by the homogenization method. Comput. Methods Appl. Engng. 153, 223–257.

Thompson, J., Soni, B., Weatherill, N., 1999. Handbook of Grid Generation. CRC Press.

Torquato, S., 1991. Random heterogeneous media: microstructure and improved bounds on effective properties. Appl. Mech. Rev. 44, 37–76.

Torquato, S., Lado, F., 1986. Effective properties of two phase disordered composite media: ii evaluation of bounds on the conductivity and bulk modulus of dispersions of impenetrable spheres. Phys. Rev. B 33, 6428–6434.

Torquato, S., Stell, G., 1983. Microstructure of two-phase random media iii. the *n*-point matrix probability functions for fully penetrable spheres. J. Chem. Phys. 79, 1505.

Willis, J., 1981. Variational and related methods for the overall properties of composites. Adv. Appl. Mech. 21, 1–78.

Zeman, J., Sejnoha, M., 2001. Numerical evaluation of effective elastic properties of graphite fiber tow impregnated by polymer matrix. J. Mech. Phys. Solids 49, 69–90.